UNIVERSIDADE FEDERAL DO RIO GRANDE DO NORTE
CENTRO DE TECNOLOGIA
PROGRAMA DE PÓS-GRADUAÇÃO EM ENGENHARIA ELÉTRICA E DE COMPUTAÇÃO

Magic Square Permutation for Photovoltaic Models Under Partial Shading

Alessandro de Souza Lima

Advisor: Prof. Dr. André Laurindo Maitelli

Co-advisor: Prof. Dr. Luciano Sales Barros

Masters Thesis presented to the Graduate Program in Electrical and Computer Engineering of UFRN (concentration area: Systems and Automation) as part of the requirements for obtaining the Master of Science degree.

PPgEEC Order Number: M558
Natal, RN, September 2019

Universidade Federal do Rio Grande do Norte - UFRN
Sistema de Bibliotecas - SISBI
Catalogação de Publicação na Fonte. UFRN - Biblioteca Central Zila Mamede

Lima, Alessandro de Souza.
Magic Square Permutation for Photovoltaic Models Under Partial Shading / Alessandro de Souza Lima. - 2019.
62f.: il.

Dissertação (Mestardo)-Universidade Federal do Rio Grande do Norte, Centro de Tecnologia, Programa de Pós-graduação em Engenharia Elétrica e de Computação, Natal, 2019.
Orientador: Dr. André Laurindo Maitelli.
Coorientador: Dr. Luciano Sales Barros.

1. Photovoltaic panel arrangements - Dissertação. 2. Partial Shading - Dissertação. 3. Reconfiguration by Magic Square - Dissertação. 4. Permutation of Magic Square - Dissertação. I. Maitelli, André Laurindo. II. Barros, Luciano Sales. III. Título.

RN/UF/BCZM CDU 621.3

Elaborado por Raimundo Muniz de Oliveira - CRB-15/429

"Don’t make a plan of fighting.That is a very good way to lose your teeth. If you try to remember you will lose! Empty your mind. Be formless, shapeless, like water. Put water into a cup, it becomes the cup. Put water into a teapot, it becomes the teapot. Water can flow or creep or drip or crash. Be water, my friend." Bruce Lee.

Acknowledgement

My family that has always been here to support me.

My professors for the corrections and ideas.

Special thanks to CAPES, for the financial support.

Abstract

Modules in a photovoltaic arrangement can receive different solar irradiation levels. This phenomenon is knowns as partial shading and causes power losses, multiple maximum power points in the power-voltage curves and overheating of the modules with lower irradiance levels. This work aims to mitigate these adverse effects using a reconfiguration method on the array based on the puzzle technique of Magic Square. Modelling of the photovoltaic modules was carried out in a MATLAB/Simulink simulation environment. The tested arrays have the total-cross-tied configuration as well as configurations meeting Magic Square criterion from the original arrangement. A permutation of the unique solution adopted was also implemented aiming a larger number of Magic Squares to observe how it behave in several shading patterns. All tests were made using up to five different levels of irradiation divided on different patterns. The Magic Square permutations presented better maximum power points on the majority of the cases, achieving more than 45% more maximum power point in two cases.

Keywords: Photovoltaic panel arrangements, partial shading, reconfiguration by Magic Square, Permutation of Magic Square.

Resumo

Módulos em um arranjo fotovoltaico podem receber diferentes níveis de irradiação solar. Esse fenômeno é conhecido como sombreamento parcial e provoca perdas de energia, múltiplos pontos de máxima potência nas curvas de tensão de alimentação e sobreaquecimento dos módulos com menores níveis de irradiância. Este trabalho visa mitigar esses efeitos adversos utilizando um método de reconfiguração no arranjo baseado na técnica de quebra-cabeça do Magic Square. A modelagem dos módulos fotovoltaicos foi realizada em ambiente de simulação MATLAB/Simulink. Os arranjos testados têm a configuração total-cross-tied e as configurações que atendem ao critério Magic Square do arranjo original. Uma permutação da única solução adotada também foi implementada visando um maior número de Magic Squares para observar como ela se comporta em vários padrões de sombreamento. Todos os testes foram feitos usando até cinco níveis diferentes de irradiação divididos em diferentes padrões. As permutações do Magic Square apresentaram melhores pontos de máxima potência na maioria dos casos, alcançando valores como 45

Palavras-chave: Arranjo de painéis solares, sombreamento parcial, reconfiguração por Magic Square, permutação de Magic Square.

Contents

List of Figures

List of Tables

List of Symbols and Abbreviations

I_0	Reverse saturation current of the diode
I_D	Current at the diode
I_P	Output current
I_R	Current in the shunt resistor
I_{0r}	Reference reverse saturation current of the diode
I_{ph}	Current generated by the cell
I_{sc}	Short circuit current
K_i	Short circuit coefficient
M	Diode ideality factor
R_S	Parasitic resistance in series
R_{sh}	Parasitic shunt resistance
S	Solar irradiance
S_r	Reference solar irradiance
T	Working temperature in Kelvin (k)
T_a	Ambient temperature
T_r	Reference working temperature in Kelvin (k)
V_P	Voltage at the terminals
V_T	Thermal potential
V_{Tr}	Reference thermal potential
k	Boltzmann constant (1.38×10^{-23} J/K)
q	Electron charge (1.6×10^{-19} C)
ε_g	Silicon energy gap

BL-HC	Bridge-linked-honey-comb
BL-TCT	Bridge-linked-total-cross-tied
CAPES	Coordenação de Aperfeiçoamento de Pessoal de Nível Superior
IMPP	Current at the maximum power point
MPP	Maximum power point
MPPT	Maximum power point tracking
MS	Magic Square
NOCT	Nominal Operating Cell Temperature
P&O	Perturb and observe
PV	Photovoltaic
SP-TCT	Series-parallel-total-cross-tied
STC	Standard temperature condition
TCT	Total-cross-tied
UFRN	Universidade Federal do Rio Grande do Norte
VMPP	Voltage at the maximum power point

Chapter 1

Introduction

1.1 Contextualization

The development of photovoltaic modules began with the discovery of Becquerel (1839), which presented a voltage resulting from the action of light in an electrolyte solution. Decades later, through new research with solid materials such as selenium, in 1914 the conversion of energy came to have an efficiency of 1%. The modern era for photovoltaics began in 1954, when Chapin used silicon in a monocrystalline cell. After technological evolution, the silicon cell under solar lighting reached 14% efficiency (Fahrenbruch & Bube 1983).

The growing interest in renewable energies has resulted in a rapid expansion of photovoltaic (PV) energy in the market. However, the power produced by photovoltaic plants depends on conditions such as temperature and irradiance (Dhimish et al. 2015).

Partial shading conditions reduces the output power from PV arrays and represents multiple Maximum Power Points (MPPs) on output characteristics (I-V and P-V characteristics) due to mismatching power losses between the PV modules. The mismatching power losses in PV systems are dependent on the shading patterns but on the shaded area, PV array topology, and physical location of the shaded PV modules in the array (Pendem, 2018). In general, multiple modules can be connected in series to increase the output voltage and in parallel to increase the output current. However, when some photovoltaic modules are shrouded by dust, shade, the total output power can be drastically reduced (Chen et al. 2013).

The conversion efficiency of a photovoltaic system is low, making it crucial to reduce losses in partial shading conditions such as passing clouds, shadows caused by buildings, trees, antennas, among others. In this context, different conventional arrangements such as total-cross-tied (TCT), bridge-link (BL) and honey-comb (HC) are used to improve system performance under shading (Yadav et al. 2017). Another different array configuration is proposed as the Vijayalekshmy et al. (2015), using the Su Do Ku logic, then the Genetic Algorithm, Deshkar et al. (2015), both in order to mitigate the losses from partial shading. The Magic Square, Yadav et al. (2017), presented a 4x4 array under shading conditions. The MS is an old puzzle known since ancient China and has a lot of different unique possible solutions depending on the MS size (Loly et al. 2009).

In addition to the importance of irradiance, temperature, and partial shading levels, the maximum power point tracker (MPPT) is important to ensure that the PV system operates

at MPP. Different types of MPPT algorithms such as pertubation and observation (P&O), incremental conductance (INC) and comparative fuzzy logic (FLC), among others, have been implemented in the past. When comparing them, it was concluded that depending on the situation, some models would be better than others in relation to response time and errors, for example (Muthuramalingam & Manoharan 2014).

In relation to the effects of shading, tests have been made with the repositioning of modules using different techniques. These techniques perform better in most cases compared to common module arrays and are a good option to reduce shading losses.

1.2 Objective

This work aims to study how the proposed 5x5 and 6x6 arrays are affected by the partial shading with up to five different levels of irradiation comparing to a classical TCT array with a reconfiguration using magic square (MS) logic.

1.3 Methodology

The methodology used in this work began in the research in articles on modeling PV modules with shading, Sharma et al. (1994) and Silvestre et al. (2009). Then, the MS logic, Yadav et al. (2017), was studied because of the possibility to reduce the shadow effect on the PV array by changing the positions of the modules. For the arrays used in this work, the methodology takes into account the other possibilities of a unique solution. The next steps were modeling the PV module, validating the model of module comparing its results to features of a commercial module. Then, the P&O and Adaptive P&O simulations are performed, as well as the standard and MS array configurations under shading. Finally, the simulations were performed, as well as the standard and MS array configurations under shading.

1.4 Text organization

The Chapter 1 is the introduction, where the PV shading is as well as the MPPT and the MS are discussed.

The chapter 2 presents the bibliographic review, showing the most important references for this work.

The Chapter 3 addresses the modeling of the solar module where the equivalent circuit is presented from equations that operate the PV cell.

The Chapter 4 presents the P&O and the Adaptive P&O MPPT, comparing the two methods showing how the parameters can influence in the results.

The Chapter 5 presents the MS logic.

Chapter 6 shows the simulations and the results based on shading tests with MS and the permutations comparing to the standard TCT configuration. The conclusion presents the work overview and implications for future research.

Chapter 2

Bibliographic review

2.1 Historic context

The sun was already used as an energy source for steam power plants in 1878 to operate steam engines, as shown in Figure 2.1. However, at the time, the cost was considered high by the French government to be considered a good investment (Kalogirou 2014).

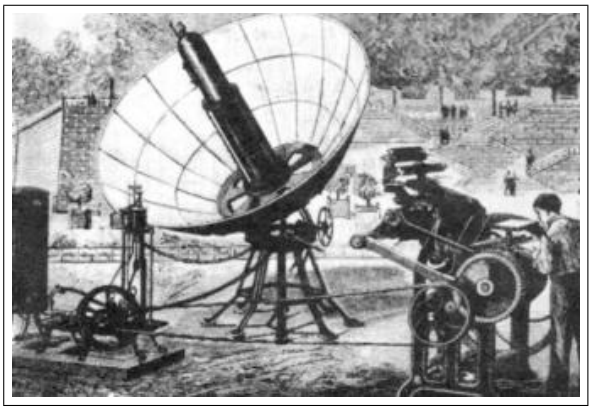

Figure 2.1: Parabolic collector powering a printing press at the 1878 Paris Exposition (Kalogirou 2014).

Later, in 1912 in Egypt, using long parabolic cylinders to focus sunlight on a tube, managing to generate 37-45kW continuously for up to 5h. However, in 1915, the plant was shut down due to World War I (Kalogirou 2014).

It has been studied from the books published by Fahrenbruch & Bube (1983) and Kalogirou (2014), as photovoltaic energy has evolved over the years through advances in materials used and also in the techniques of how to obtain solar energy.

2.2 Limitations and benefits

Photovoltaic energy has some limitations, the most obvious of which is that it can only be captured during the day. It is not a suitable source of energy in regions where there

are unstable weather conditions. Long exposure to exhaust gases from cars and aerosol reduces the current of silicon PV cells by 10% and 7% respectively. Another important issue concerns the space to install a plant, for example, to produce 1MW using crystalline modules (the commercial ones have 18% efficiency) requires about $16.187m^2$ of space (Kabir & Kumar 2018).

Among the main benefits, there is no noise generation because there are no mechanical parts that move. In addition, it can be installed easily on the roofs of buildings or even mounted on walls, giving flexibility in the way of installation. They have lower chances of large-scale failures, as the modules are distributed individually in arrangements, one part can function without the need for another. New panels can be added later to the arrangements to increase the power generation capacity (Kabir & Kumar 2018).

2.3 PV cell modeling

The Trejos-Grisales et al. (2015), use the PV model taking into account the inflection points and bypass diodes activation, which are usually due to partial shading. In this method, there is a bigger focus on the mathematical approach than to the circuits. The Chen et al. (2013) PV model uses a digital signal processing method to emulate two photovoltaic modules under partial shading in parallel and series configuration. Simpler than the DSP method, the modeling of the panels was based on Nguyen (2015) which presents the cell model using a diode. The model has an equivalent circuit, with a current source representing the photoelectric current, series resistance, and shunt resistance. From the circuit, the equations of the model are obtained. In practice, the cells are grouped in large quantities that can be called modules and these modules, when connected in series or parallel, create PV arrays. The article also analyses how shadowing conditions can influence power-voltage curves.

2.4 Shading and bypass diode

When a PV cell is shaded, it behaves like a charge. In Sharma et al. (1994), shows that adding a by-pass diode in parallel with each cell can reduce losses due to shading, because the diode gives a possible path to the current due to the low resistance. In the work of Silvestre et al. (2009), shadowing simulations and the use of the by-pass diode is performed, where each diode is connected in parallel to a module. In Kardi et al. (2012), shading tests are performed using series and parallel configurations, varying the number of cells and the solar irradiation. In Chen et al. (2013), it is observed that when using diodes in parallel with the PV modules multiple points of maximum power can occur. A method to reduce shading losses is proposed in Castelano et al. (2015), taking into account the size of the module, the location of the installation and the angulation of the PV module.

2.5 MPPT

The maximum power point tracking (MPPT) is important to ensure the PV system operating at the maximum power point (MPP). Different types of MPPT algorithms such as perturb and observe (P&O), incremental conductance (INC), and comparative fuzzy logic (FLC), among others, have been implemented in the past. Due to the great MPPT variety, researchers have compared techniques to obtain the best possible method for conditions such as time response, efficiency, complexity and implementation cost (Muthuramalingam & Manoharan 2014).

2.6 Main methods/techniques used to reduce the effects of shading

The Pendem & Mikkili (2018) investigates the performance of different array typologies under various shading patterns, analyzing the performance with respect to open-circuit voltage, short-circuit current, global maximum power point (GMPP) and others. It was observed that the TCT array generates the maximum power by mitigating the mismatching power losses. Vijayalekshmy et al. (2016) present a novel TCT configuration called Optimal TCT, presenting an improved performance regardless of the complexity as the array size increases, involving a larger number of constraints. In Bosco & Mabel (2017), different configurations are proposed using a cross diagonal view matrix, consisting of changing the physical location of the module without changing the electrical circuit. The work presented a better power output on the partial shading tests made. In Vijayalekshmy et al. (2015) it presents modules replacement according to Su Do Ku logic where simulations results were better than for the original configuration. Deshkar et al. (2015), presented a Genetic Algorithm based reconfiguration scheme for the arrangement of PV modules in a PV array. In this case, the electric interconnections are changed, while the module position is maintained. The system performance presented superior results under shading conditions than the Su Do Ku arrangement. In the practical test of Malathy & Ramaprabha (2018), the proposed static architecture to negate the impact of partial shading under non-uniform irradiation conditions. They conclude that the use of sensors, switches and sophisticated control algorithms to modify the interconnections are not the best choice for large scale installations, by reducing the reliability of the overall system while increasing the complexity. The proposed static configuration presented a simple, lucrative, and cost-effective solution for small residential installations under partial shading conditions. Yadav et al. (2017), which studies the modules changing location following a similar logic as above, which is called Magic Square (MS).

Then from the information gathered in the articles and books studied, the modules are modeled following the model of a cell. Subsequently, the MS is studied including the permutation of the configurations to study how they perform under several different shading effects compared to the standard TCT array.

Chapter 3

Solar module

This chapter presents the modeling of a photovoltaic cell from mathematical equations that define its operation. Then, the data of a commercial module applied to the model, is validated through a current-voltage curve.

3.1 Modeling the solar cell

The modeling of the PV module was based on Nguyen (2015), which presents the cell model using a diode. The model has an equivalent circuit, with a current source representing the photoelectric current, series resistance and shunt resistance presented in Figure 3.1. From the circuit, the model equations are defined. In practice, the cells are grouped in large quantities that can be called modules and these modules, when connected in series or parallel, originate PV arrays.

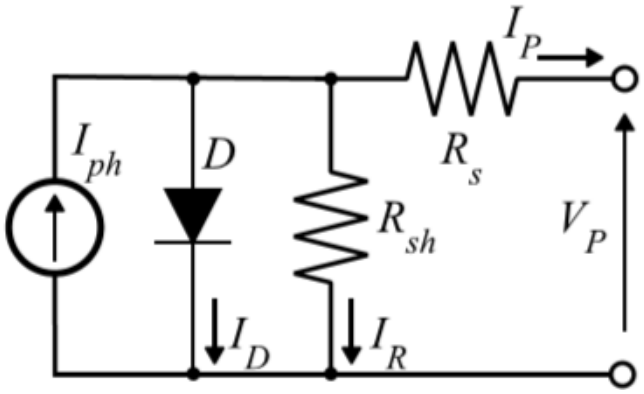

Figure 3.1: Equivalent circuit for a PV cell.

$$I_P = I_{ph} - I_D - I_R. \tag{3.1}$$

Where:

- I_P is the output current;

- I_{ph} is the photoelectric current;
- I_D is the current in the diode;
- I_R is the current in the shunt resistor.

$$I_{ph} = \frac{S}{Sr}(I_{sc} + K_i(T - T_r)). \tag{3.2}$$

Where:

- S is the solar irradiance;
- S_r is the reference solar irradiance;
- I_{sc} is the short circuit current;
- K_i is the short circuit coefficient;
- T is the working temperature in Kelvin (k);
- T_r is the reference working temperature in Kelvin (k).

Thus, only irradiance and temperature can cause variations in the generated current, since the other terms are constant, depending on the material composition. The I_D is represented by (3.3).

$$I_D = I_0(e^{\frac{V_P + R_S I_P}{mV_T}} - 1). \tag{3.3}$$

Where:

- I_0 is the reverse saturation current of the diode;
- V_P is the voltage at the terminals;
- M is the diode ideality factor;
- R_S is the parasitic resistance in series;
- V_T is the thermal potential.

Equation (3.4) is a current divider, where $R_{sh}$is the parasitic shunt resistance, which has a value larger thanR_S .

$$I_0 = I_{0r}\frac{T^3}{T_r}e^{(\frac{\varepsilon_g}{m}(\frac{1}{V_{Tr}} - \frac{1}{V_T}))}. \tag{3.4}$$

Where:

- ε_g is the silicon energy gap;
- I_{0r} is the reference reverse saturation current of the diode;
- V_{Tr} is the reference thermal potential.

For the T calculation, in (3.5) the T_a represents the ambient temperature and NOCT that means (Nominal Operating Cell Temperature), which is the nominal temperature condition for the environment of 20^0 C.

$$T = T_a + S(\frac{NOCT - 20}{800}). \tag{3.5}$$

The values of I_{0r} and ε_g are defined in (3.6) and (3.7) respectively. In (3.8) the formula of V_T is presented.

$$\varepsilon_g = \varepsilon_{gr} - 7.02 \times 10^{-4}\left(\frac{T^2}{1108+T}\right); \tag{3.6}$$

$$I_{0r} = \frac{I_{sc}}{e^{\left(\frac{V_{oc}}{mV_{Tr}}\right)-1}}; \tag{3.7}$$

$$V_T = \frac{kT}{q}. \tag{3.8}$$

Where:

- k is the Boltzmann constant (1.38×10^{-23} J/K);
- q is the electron charge (1.6×10^{-19} C).

The equations (3.1), (3.2), (3.3), (3.7), (3.8) and (3.9) were implemented in Matlab/Simulink through blocks with the intention of applying them in the equivalent circuit of the cell. The Figure 3.2 shows the block of the PV module used for the simulations. The ambient temperature was set to 25.

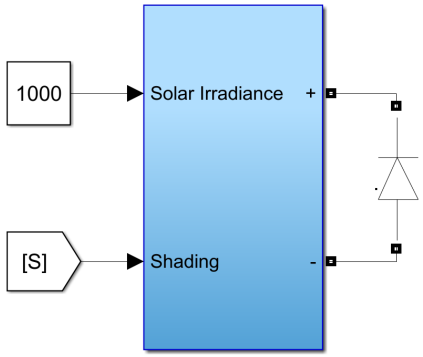

Figure 3.2: PV module block.

As shown in Figure3.2, the module has two inputs, where the first one is the solar irradiance, while the second represents the shading coefficient. For the modeling of the equivalent circuit shown in Figure 3.1, the generated current I_{ph} is subtracted by the current I_D and outputs the current I. It is multiplied by the shading coefficient, which is assigned values between 0 and 1. So, when the module is totally shaded, the coefficient, it doesn't contribute to the generation of electricity. From the I_{ph}-I_D output multiplied by the shadow coefficient; this value is connected in a current-controlled current source. The two resistors R_S and R_{Sh} are present in the equivalent circuit, while the voltage value above the R_{sh} is measured for the calculation of V_{sh} which is important for the calculation of the current I_D. In the output, the poles of the module are used for their connection.

For each module, a diode called the by-pass diode was added. This addition is important to bypass the module when shading occurs (Ishaque & Salam 2013).

3.2 PV cell, module and array

The PV module is done by connecting several amount of PV cells in series and/or parallel. By doing this, the small amount energy produced by the PV cells is compensated.

Supposing that the PV cell is shown in Figure 3.3(a) has a nominal power output of 5 watts, then, the PV module having the 36 modules connected in series Figure 3.3(b) has 180W of nominal power output. Thus, the series array has 720W Figure 3.3(c) of power output.

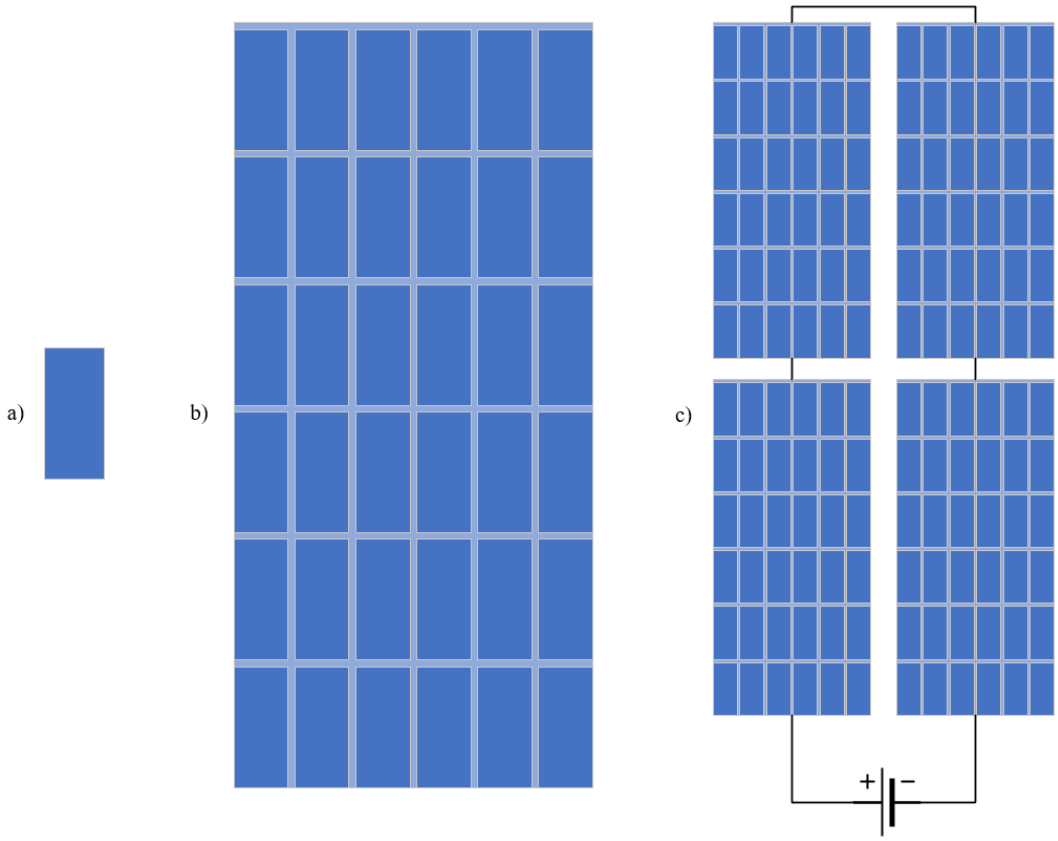

Figure 3.3: Graphic demonstration of cell, module and array; a) PV cell; b) PV module; c) PV series array.

The power generated by the cell, the number of the cells per module are defined by the manufacturers and exist a vast number of possibilities.

Chapter 4

MPPT P&O and Adaptive P&O

This chapter presents the MPPT P&O. In order to show the efficiency of the algorithms, a comparison is made between the MPPT P&O and Adaptive P&O through a simulation where one of the modules is shaded at a given moment and then the shading is removed.

4.1 MPPT P&O

From the equations that define the operation of the solar panel given in Chapter 3, it is possible to simulate the MPPT working.

The MPPT P&O (Perturb & Observe) is an algorithm that applies a small voltage variation and verifies the power variation. If there is an increase in the power supplied by the array, the algorithm follows with perturbances in the same direction. However, if there is a decrease in power, in the following iteration, the disturbance will occur in the opposite direction. The algorithm used is shown in Figure 4.1 (Villalva & Ruppert 2009).

4.2 MPPT efficiency

Two modules were placed in series, while the top module being shaded in a time equal to ten seconds, then withdrawing the ten seconds later. The total time for this simulation was 30 seconds. The blocks used are shown in Figure 4.2. The shading test for the MPPT P&O was performed as follows. The two modules initially receive 1.000 W/m^2 of irradiance. The top module has for input two steps with values equal to 1.000, with step 1 entering at 10 seconds and the second at 20 seconds. The block named as S is the MPPT step.

In Figure 4.3 it is observed that from the shading, for 3.1 seconds, there is a delay caused by the P&O. It is also possible to see that when the shading is removed at 20 seconds, the time for the total power generated by the modules to reach the steady-state value is 4 seconds. In Figure 4.4 it is possible to observe in the steady-state (from 24 to 25 seconds) that the power, voltage, and current almost don't vary.

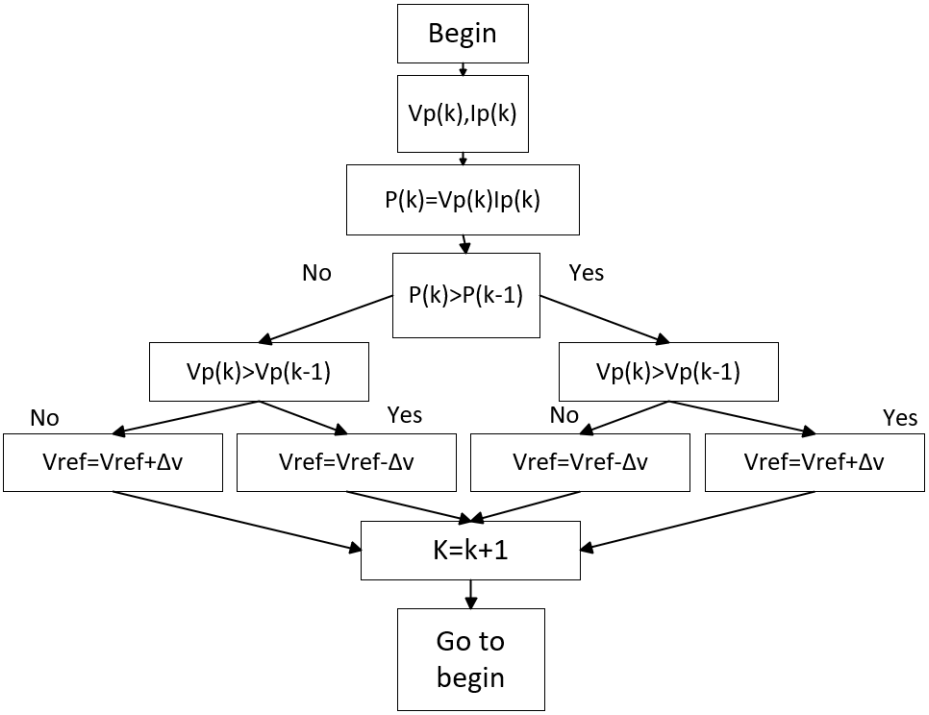

Figure 4.1: Maximum power point tracking perturb and observe.

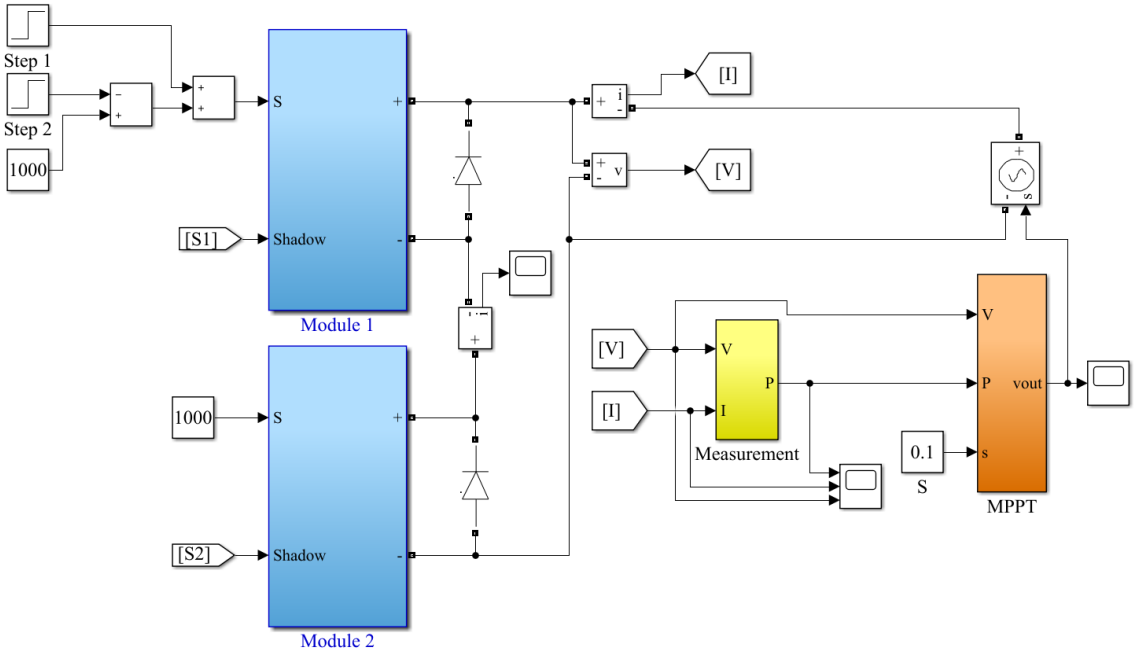

Figure 4.2: Configuration used for the MPPT test.

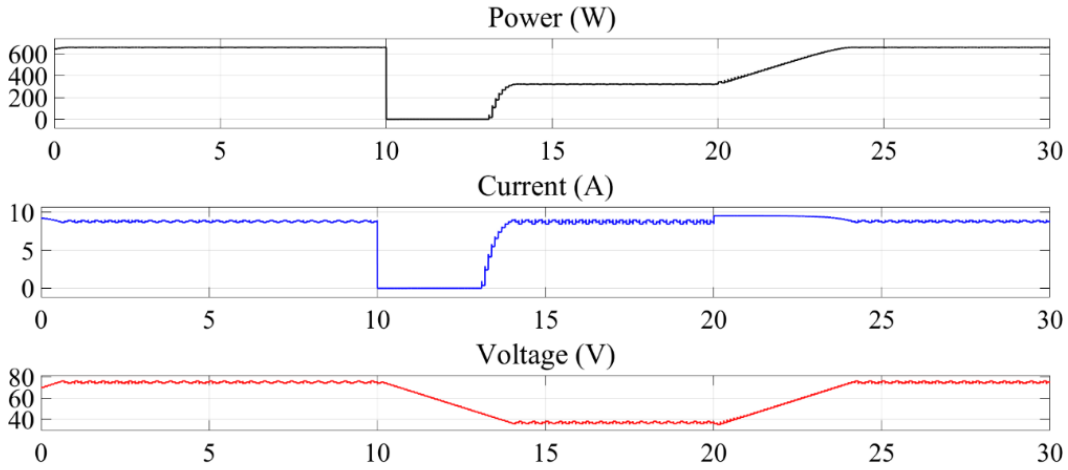

Figure 4.3: MPPT P&O first test.

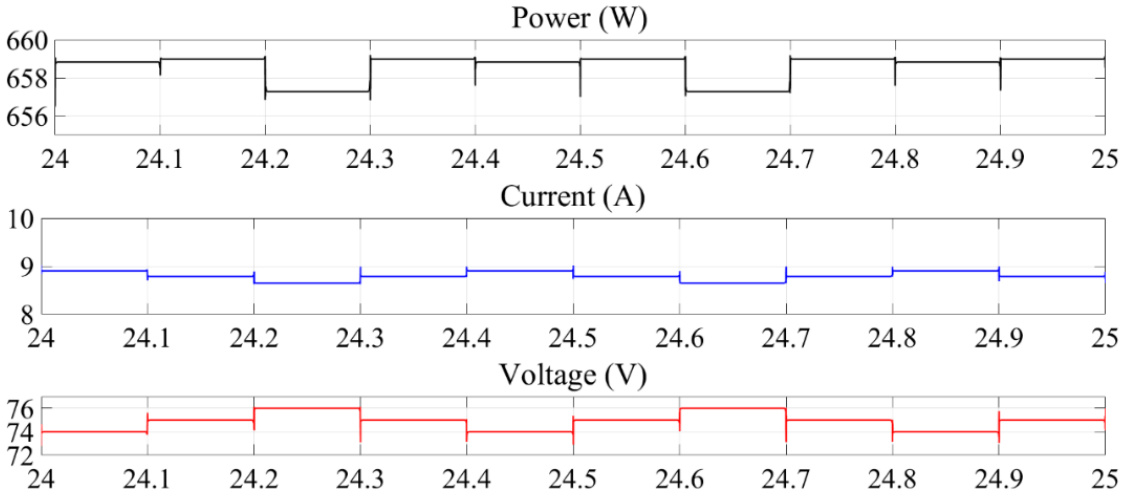

Figure 4.4: MPPT P&O first test zoom.

By changing the MPTT P&O step to a bigger value, the time between the occurrence of the shadow and the stabilization is minimized, however, the ripple is increased, shown both on Figure 4.5 and Figure 4.6.

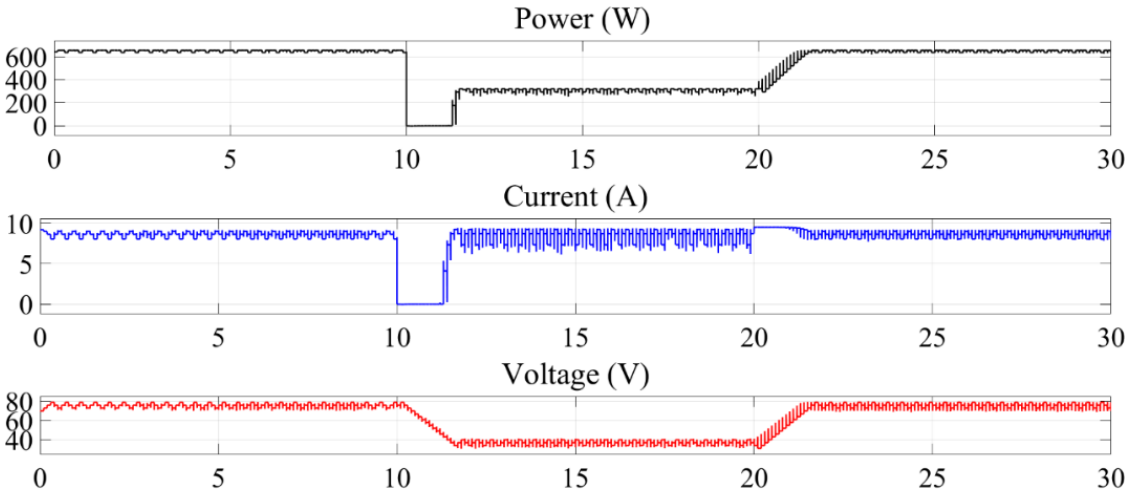

Figure 4.5: MPPT P&O second test.

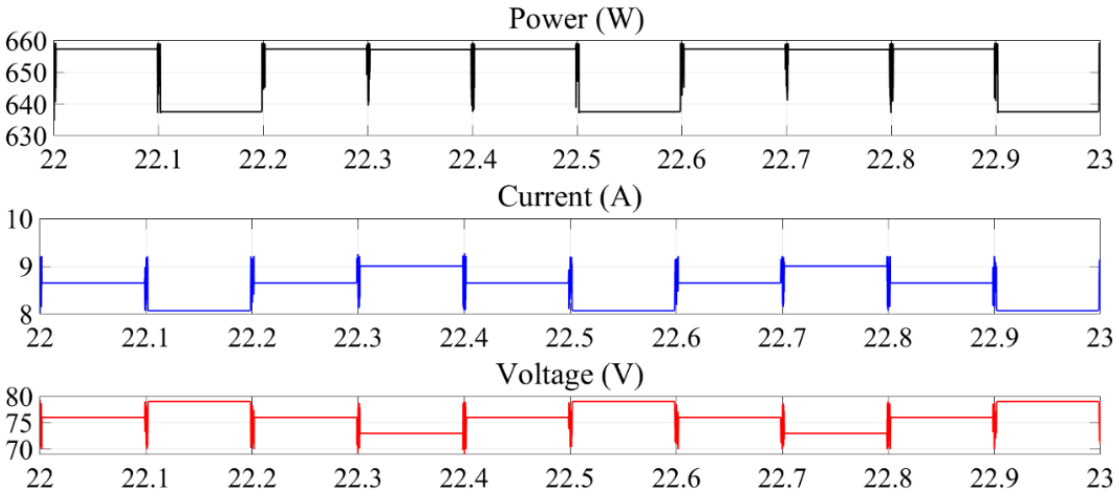

Figure 4.6: MPPT P&O second test zoom.

In order to optimize the response time and the ripple of the MPPT P&O, an Adaptive P&O was implemented, which has an adjustable gain. Like the standard P&O, the Adaptive P&O reads and compares current and previous voltage and power values, as well as uses a fixed-step. However, in addition to the fixed step, there is an adjustable step that

varies as needed. When there is shading or withdrawal, it should add the adjustable step to the fixed step, to stabilize the system more quickly.

After implementing the Adaptive P&O, the same system was simulated again and under the same conditions shown in Figure 4.7 and Figure 4.8.

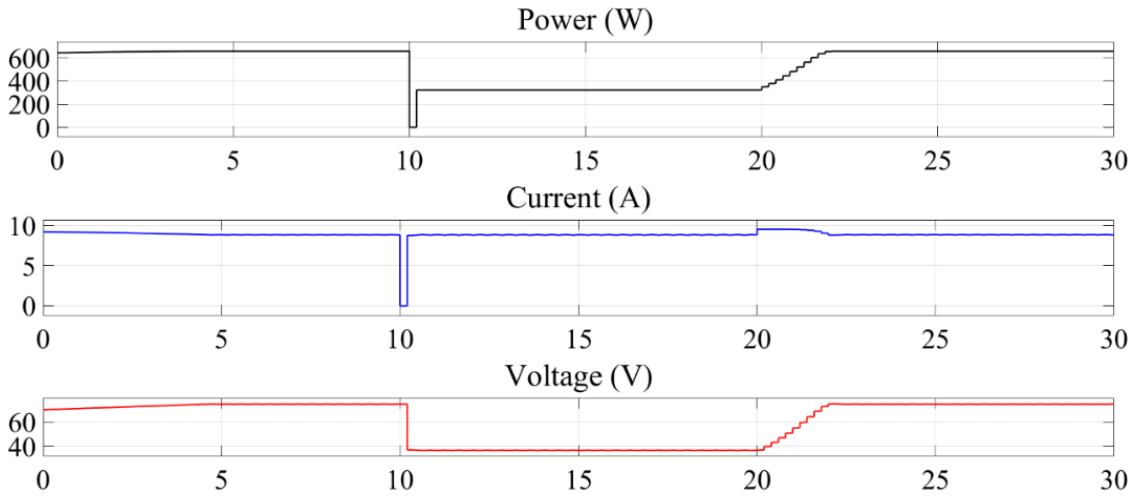

Figure 4.7: Adaptive P&O test.

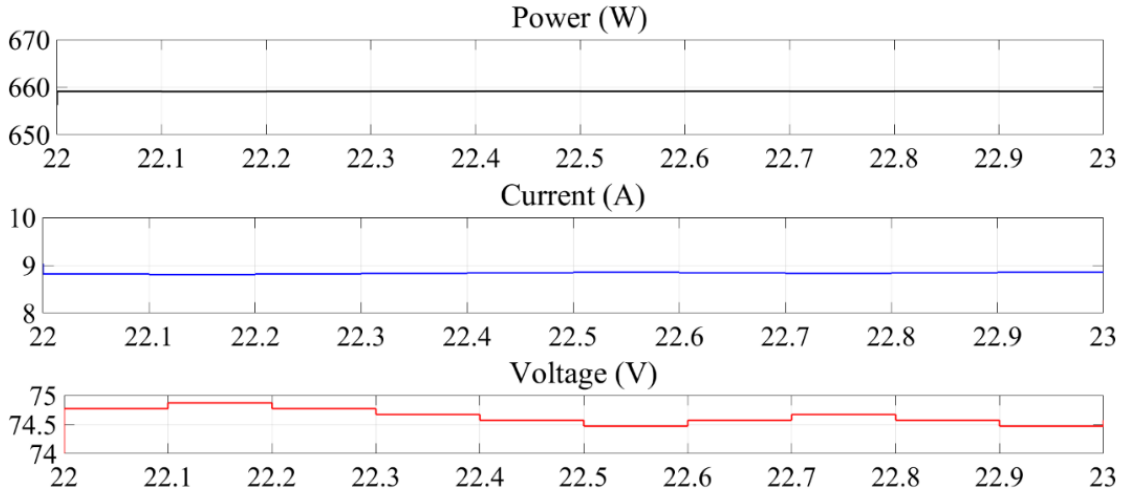

Figure 4.8: Adaptive P&O test zoom.

In the simulation shown in Figure 4.7, it can be observed that the Adaptive P&O method is faster and has a lower noise level than in the simulation shown in Figure 4.5. In the first moment, the delay caused by the MPPT is much smaller, because, at 10 seconds the system remains without output power for only 0.2 seconds, compared to the previous

method that lasted 3.1 seconds. In the second moment, the system takes 2 seconds to stabilize and compared to the previous method. The Adaptive P&O was able to perform the same task in half the time besides presenting a smaller ripple.

Chapter 5

Magic Square

The chapter initially introduces the definition of MS. Then, two different MS sizes are presented, one 4x4 and a 5x5, including a permutation on the arrays maintaining the original MS characteristics.

5.1 Magic Square definition

Magic square is a puzzle that defines the placements of numbers based on logic. It consists of a nxn matrix where the sum of all number in a row, column or diagonal results in a same value called magic number. The magic number M can only be obtained from a magic square of order 3 or larger (5.1).

$$M = \frac{n(n^2+1)}{2}. \tag{5.1}$$

The first known magic square is called Lo Shu shown in Figure 5.1, the magic number for a 3x3 magic square is 15. There is only one unique solution for this puzzle, while others solutions are obtained just from rotation or reflection of this original solution, reaching total of 8 possibilities.

Another famous magic square is the Albrecht Durer‘s 4x4 shown in Figure 5.2 being an order 4 magic square, and the magic number is 34. But besides other characteristics common to magic squares, it has the bottom row the number 1514, which is the year that the puzzle was made.

Bessy (1699) presented the 880 unique magic squares of order four. Schroeppel (1976), found that there are 275.305.224 unique 5x5 magic squares. The number of 6x6 magic squares is not known exactly, but Pinn & Wieczerkowski (1998) using the Parallel Tempeering Monte Carlo method found that there is approximately $(1.7745 \pm 0.0016)10^{-19}$ different solutions (Table 5.1).

5.2 5X5 Magic Square

Calculating the magic number for the 5x5 MS.

4	9	2	8	1	6	2	9	4	6	1	8
3	5	7	3	5	7	7	5	3	7	5	3
8	1	6	4	9	2	6	1	8	2	9	4
4	3	8	2	7	6	8	3	4	6	7	2
9	5	1	9	5	1	1	5	9	1	5	9
2	7	6	4	3	8	6	7	2	8	3	4

Figure 5.1: Lo-Shu magic square all eight possibilities.

16	3	2	13
5	10	11	8
9	6	7	12
4	15	14	1

Figure 5.2: Albrecht Durer‘s 4x4 magic square.

Table 5.1: Magic Square Solutions

Magic Square Size	Unique Solutions	Total Solutions
3x3	1	8
4x5	880	7040
5x5	275,305,224	2,202,441,792
6x6	$(1.7745 \pm 0.0016)10^{-19}$	$8(1.7745 \pm 0.0016)10^{-19}$

$$M = (\frac{5(5^2+1)}{2}). \tag{5.2}$$

For a 5x5 MS, the magic number M is equal to 65, so all the rows, columns and diagonals by summing its values have 65 as shown in Figure 5.3. The standard TCT is shown in Figure 5.3.

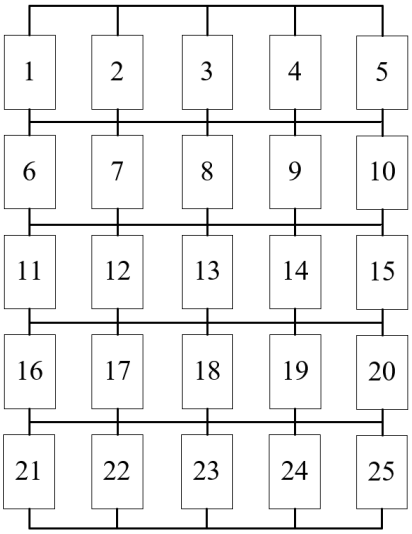

Figure 5.3: Standard 5x5 TCT array configuration.

It is possible to obtain these solutions by rotating the module positions on the MS1 array Figure 5.4(a). The other seven solutions are obtained by reflecting vertically Figure 5.4(b), horizontally Figure 5.4(c), horizontally then vertically Figure 5.4(d), transposing Figure 5.5(a), transposing then reflecting vertically Figure 5.5(b), transposing then reflecting horizontally Figure 5.5(c), transposing then reflecting horizontally and vertically Figure5.5(d).

Comparing the standard TCT shown in Figure 5.3, and the MS logic shown in Figure 5.4(a), the module 1 is physically located where originally module 3 was. Module 2 is physically located where module 24 is on the standard TCT configuration, and so on. In this way, the arrangement of PV modules is meeting the requirements of the magic square. Thus, when a shading occurs in some regions of the array, there is a great possibility that the MS technique obtains smaller losses due to the spacing of the modules.

To confirm that the array from Figure 5.4 is a MS, the equations from (5.3) to (5.14) are presented.

The sum of rows is made from (5.3) to (5.7), the sum of columns from (5.8) to (5.12) and for diagonals (5.13) to (5.14).

$$17+24+1+8+15=65. \tag{5.3}$$

$$23+5+7+14+16=65. \tag{5.4}$$

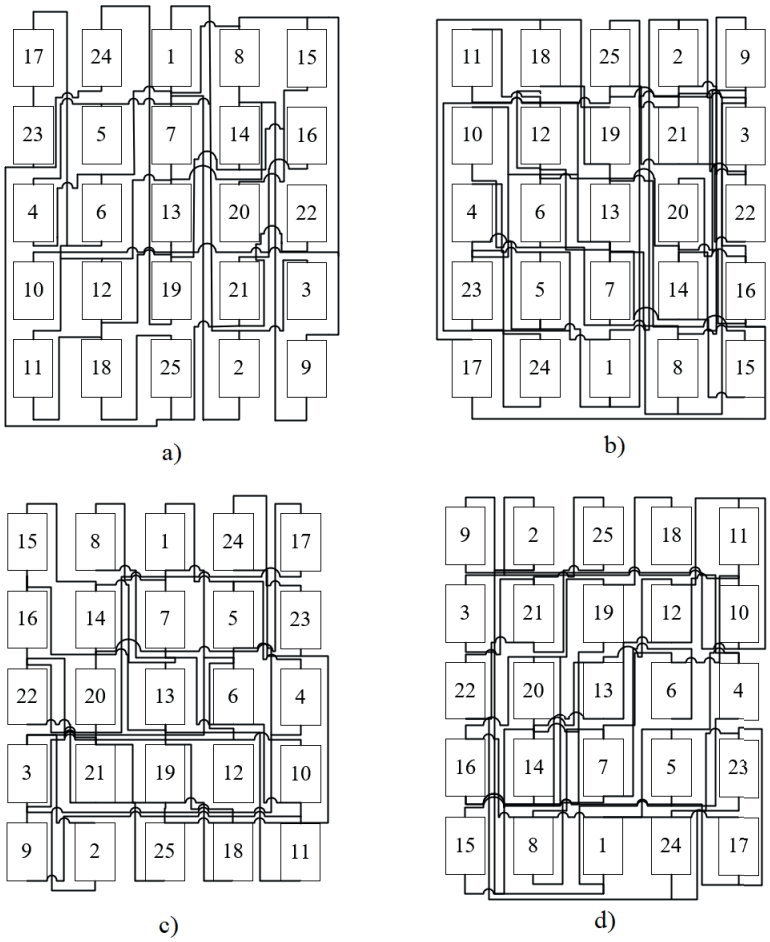

Figure 5.4: Magic Square 5x5 rotations: a) MS1; b) MS2; c) MS3; d) MS4.

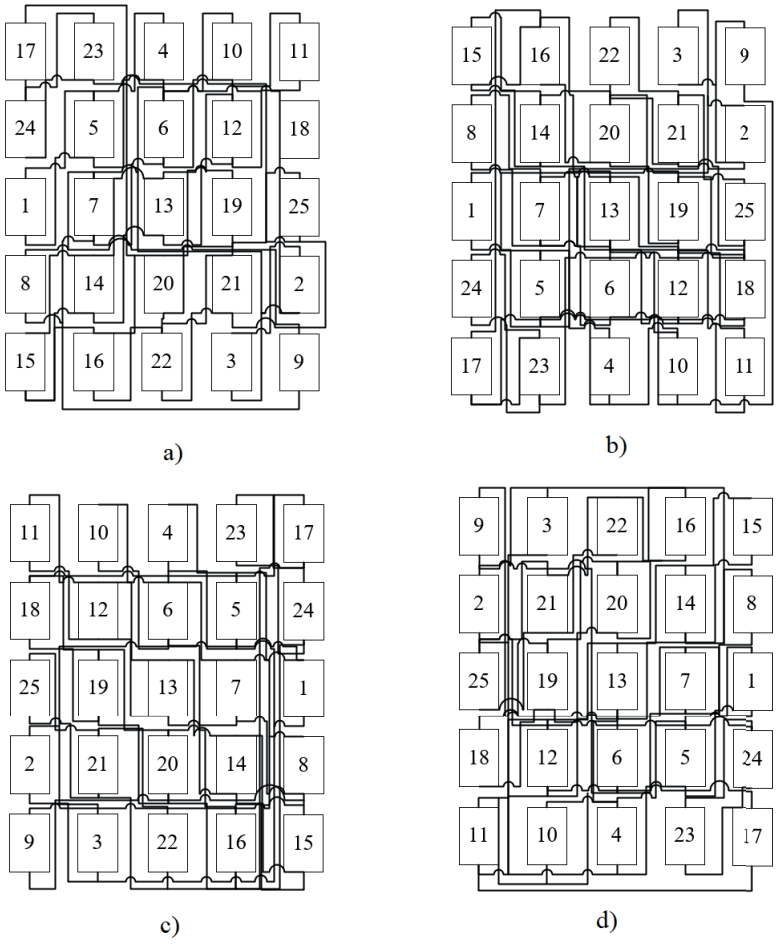

Figure 5.5: Magic Square 5x5 rotations: a) MS5; b) MS6; c) MS7; d) MS8.

$$4+6+13+20+22=65. \tag{5.5}$$

$$10+12+19+21+3=65. \tag{5.6}$$

$$11+18+25+2+9=65. \tag{5.7}$$

$$17+23+4+10+11=65. \tag{5.8}$$

$$24+5+6+12+18=65. \tag{5.9}$$

$$1+7+13+19+25=65. \tag{5.10}$$

$$8+14+20+21+2=65. \tag{5.11}$$

$$15+16+22+3+9=65. \tag{5.12}$$

$$17+6+13+21+9=65. \tag{5.13}$$

$$11+12+13+14+15=65. \tag{5.14}$$

5.3 6x6 Magic Square

Calculating the magic number for the 6x6 MS.

$$M=(\frac{6(6^2+1)}{2}). \tag{5.15}$$

For a 6x6 MS, the magic number M is equal to 111, so all the rows, columns and diagonals by summing it‘s values have 111 as shown in Figure 5.7 and Figure 5.8. The standard TCT is shown in Figure 5.6.

As well as the 5x5 MS, the 6x6 MS rotations are made in the same way and these are the 6x6 MS arrays tested in this work in comparison with a classical TCT arrangement under shadow conditions. All of the MS arrays have the same magic number M Figure 5.6.

The only difference between the standard and the MS array is the physical position. For example, in the MS array, the module numbered as 1, is physically on the position of module 36. But electrically, these modules are at the same position as the standard array. For module 1, the top and bottom connections are respectively linked to the top and bottom connections for modules 2, 3, 4 ,5, and 6, as well as for the standard array. The module 1 bottom connection is linked to the top connections of modules 7, 8, 9, 10, 11

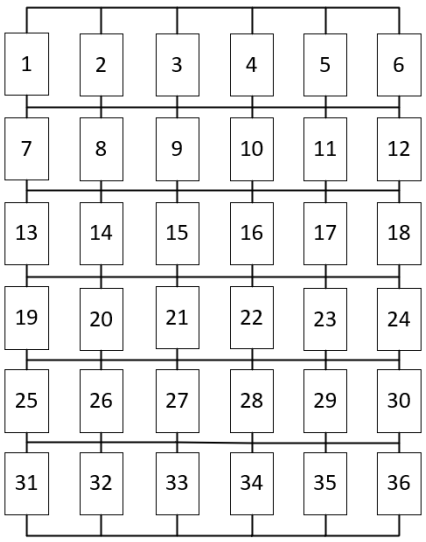

Figure 5.6: Standard 6x6 TCT array configuration.

and 12, as well as for the standard array. For the other modules, the same idea is used to guarantee that the connections are the same for both standard and MS configurations.

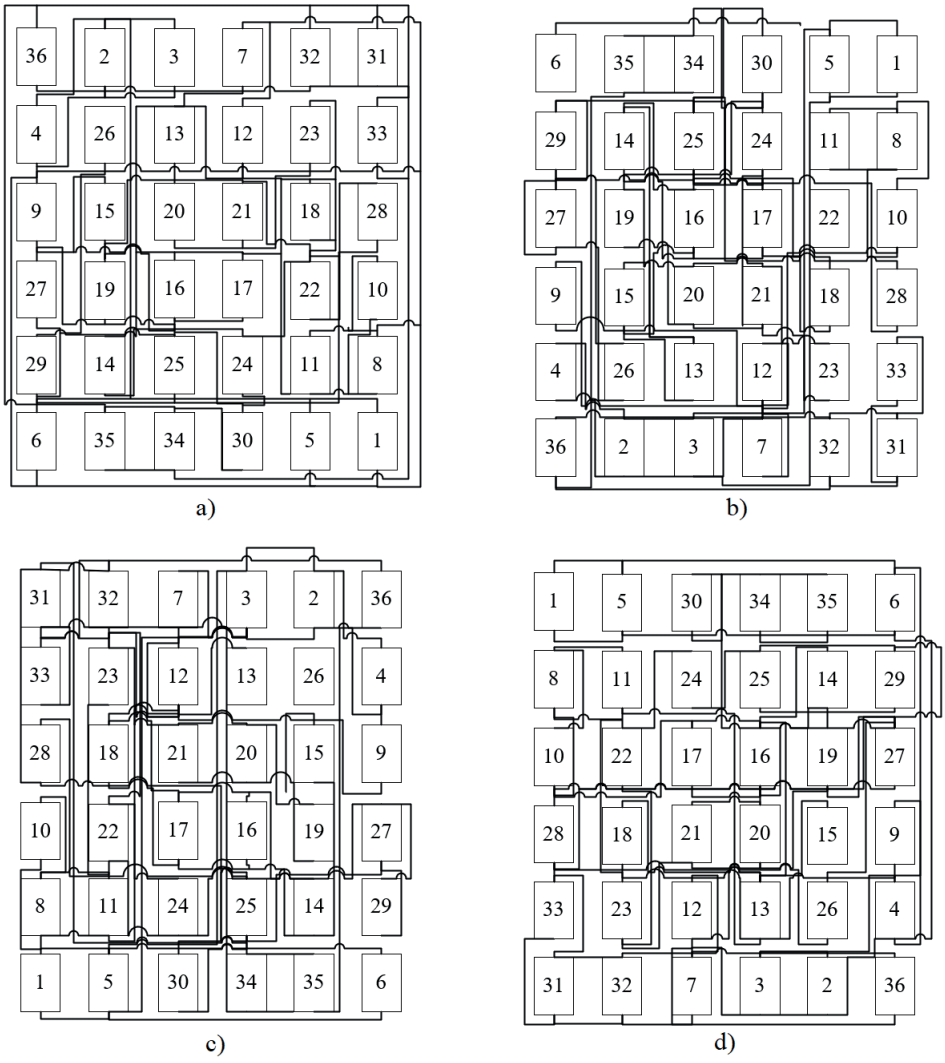

Figure 5.7: Magic Square 6x6 rotations: a) MS1; b) MS2; c) MS3; d) MS4.

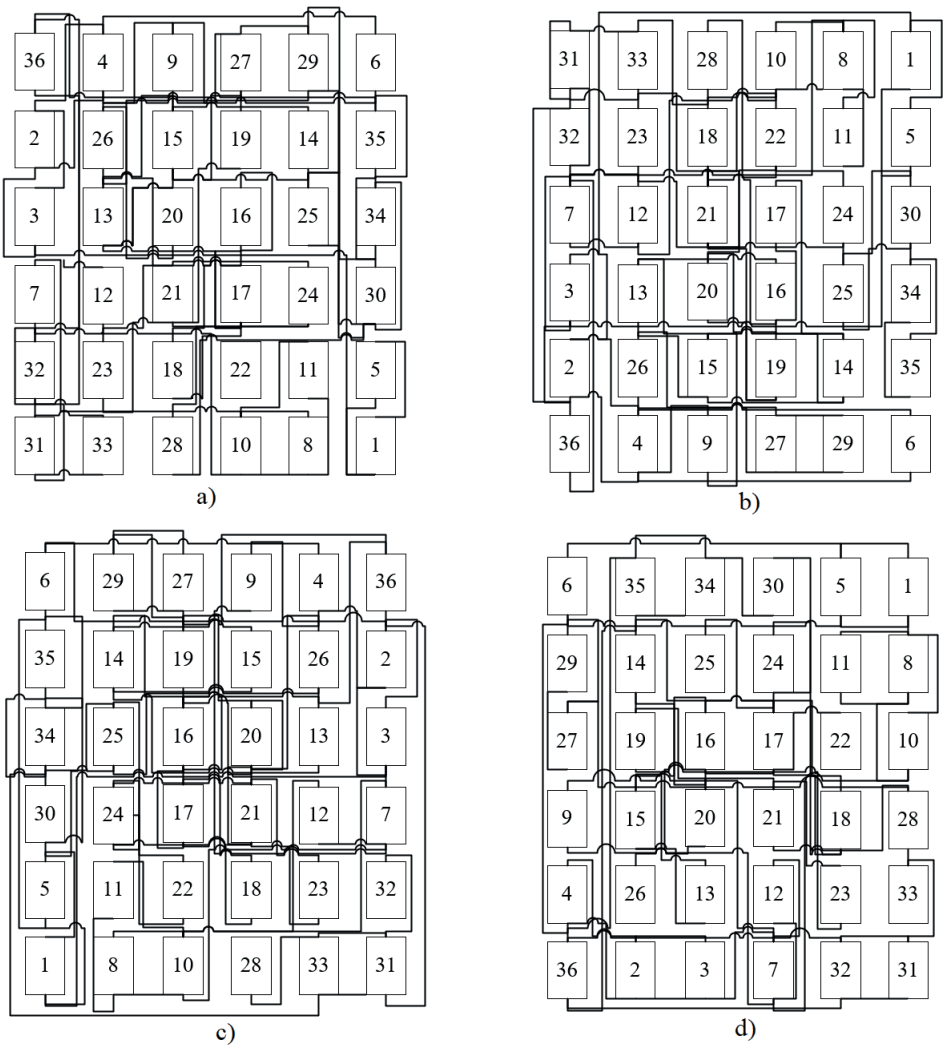

Figure 5.8: Magic Square 6x6 rotations: a) MS5; b) MS6; c) MS7; d) MS8.

Chapter 6

Simulations and results

When proposing a rearrangement of the PV array, the MS aims to isolate the shading points so that their effects are minimized. In order to mitigate the losses caused by shading, the MS logic can be implemented so that a given shading causes fewer losses than a conventional module configuration.

As shown in Chapter 3, the irradiance variation has great relevance in relation to the generation of PV energy. It can be caused by shading due to clouds, some building neighboring, or even dirt in the modules that can decrease the power generated. The shading patterns tested are shown below.

6.1 PV module features

The parameters for each module were based on a commercial solar module from Canadian Solar company of 330W. The datasheet information is presented on Table 6.1. Where STC stands for standard temperature condition.

6.2 Validating the model modelled

The modelled module has its operating characteristic shown in Figure 6.1 and Figure 6.2.

In Figure 6.1, it is possible to find the value of the short circuit current and the open-circuit voltage. The first occurs when the voltage has zero value, while the second one is found when the current equals zero. In Figure 6.2 it is possible to find the maximum power point MPP.

From the commercial module data-sheet, the current-voltage curve is presented in Figure 6.3, which corresponds to the model CS6U-335M, the model closest to the C6SU-330M that was used in this work.

It is concluded that the module modelled from the mathematical equations presented in this chapter has approximate values in relation to the current-voltage curves of the commercial module data-sheet. Therefore, the model is valid for module arrangements and partial shading tests.

Table 6.1: Canadian Solar 330W module datasheet.

STC (1000W/m^2, 25^{o}C)	
Nominal max. power	Max.330 W
Operating voltage	37.2 V
Operating current	8.88 A
Open circuit voltage	45.6 V
Short circuit current	9.45 A
Number of cells	72
NOCT (800 W/m^2, 20^{o}C)	
Nominal max. power	239 W
Operating voltage	33.9 V
Operating current	7.05 A
Open circuit voltage	41.9 V
Short circuit current	7.66 A
Number of cells	72

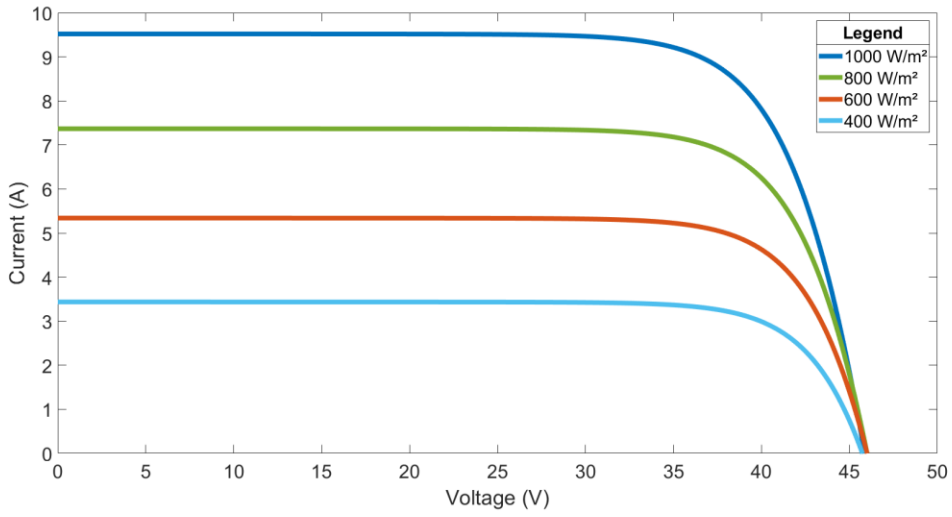

Figure 6.1: Voltage-current curves varying irradiance from 100W/m^2 to 1000W/m^2.

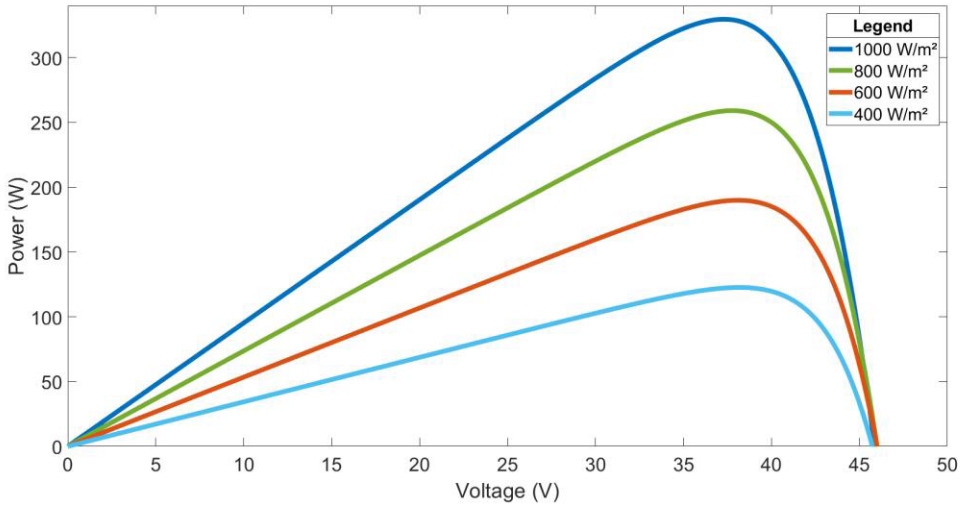

Figure 6.2: Voltage-power curves varying irradiance from 100W/m^2 to 1000W/m^2.

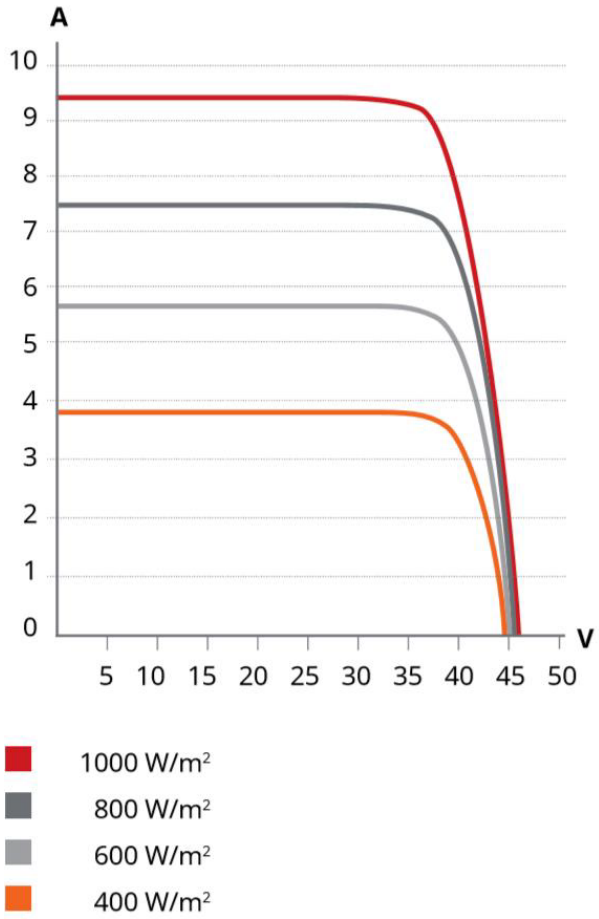

Figure 6.3: Voltage-current curve (Canadian Solar datasheet).

6.3 5x5 Shading tests

The arrays from Figure 5.4, and Figure 5.5 are tested by different shading patterns shown in Figure 6.4. The chosen irradiance level was 1000W/m^2 for the non-shaded modules colored in white. The shaded modules are the grey colored ones and receive 0W/m^2 of irradiance. The module temperature for both situations was set to 25ºC. For example, in the first shading pattern, Figure 6.4.(a), the four modules shaded for the standard array of Figure 5.3 are the modules 1, 2, 6 and 7. However, for the MS1 configuration from Figure 5.4(a), the shaded ones are 5, 17, 23, 24. For the other seven MS arrays, different modules are shaded. This logic applies to all shading patterns shown in Figure 6.4.

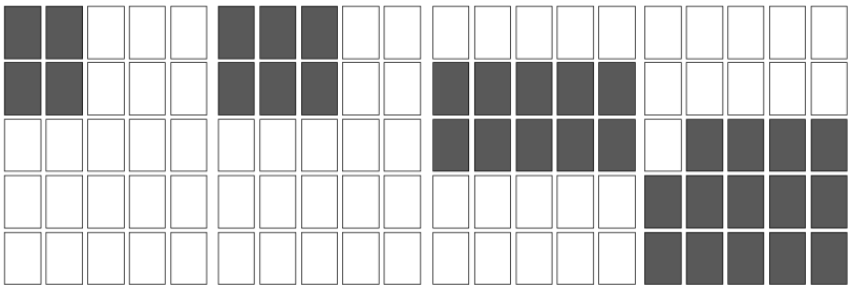

Figure 6.4: The shading patterns tested. a) Shadow pattern 1; b) Shadow pattern 2; c) Shadow pattern 3; d) Shadow pattern 4.

6.4 6x6 Shading tests

The simulation was done using Matlab/Simulink where the arrangement has a bypass diode per module as well as the model shown in Section 3.1. To better understand how the permutated MS and classic configuration behave, eight different shadow patterns were implemented, as shown in Figure 6.5. The shadings were defined arbitrarily and have five levels of irradiance, with 0 W/m^2, 200 W/m^2, 600 W/m^2 and 1000 W/m^2. For all tests shown in Figure 6.5, the module temperature was set to 25ºC.

6.5 Simulations and results for 5x5

In shadow pattern 1, the power per voltage response given as in Figure 6.6. It can be observed that the MPP levels are slightly larger for MS configurations compared to the standard. In this case, comparing to the original configuration, the MS1 instead of shading modules 1, 2, 6, and 7, the modules 17, 23, 25, and 5 were shaded. The MPP reached by the MS was 5655W, whereas for the original configuration it was 5472W.

The shadow pattern 2 is simulated when shading 24% of the modules, as can be shown in Figure 6.7. In this case, it can be clearly seen that the use of the settings with MS are more efficient than the standard setting, reaching up to 45.5% more of MPP. The MPP

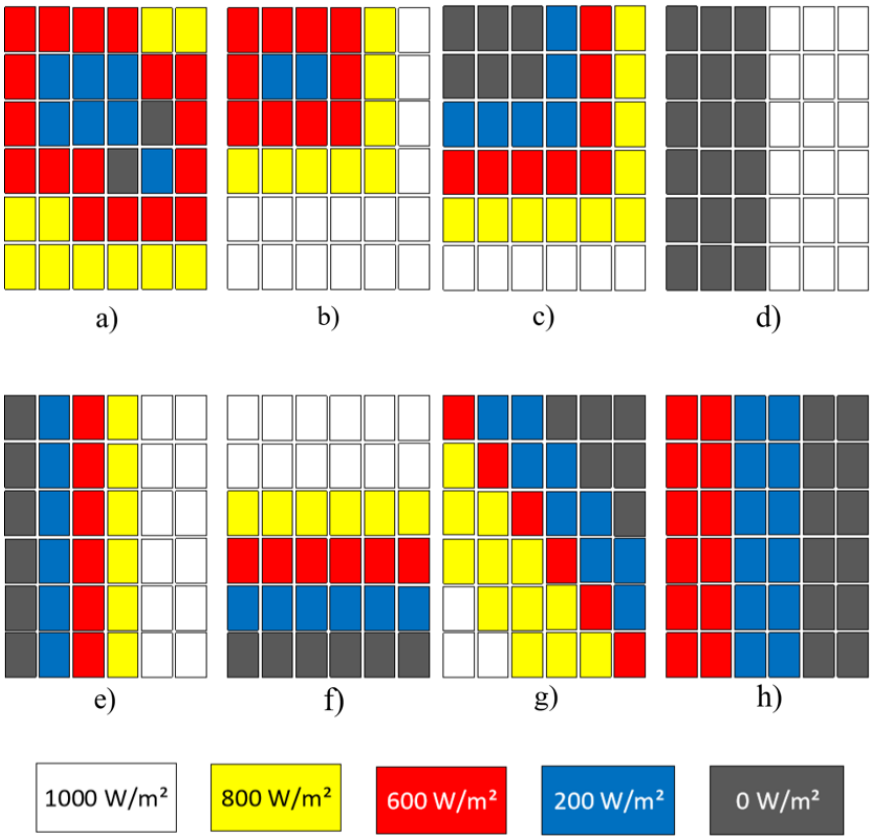

Figure 6.5: The shading patterns tested. a) S1; b) S2; c) S3; d) S4; e) S5; f) S6; g) S7; h) S8.

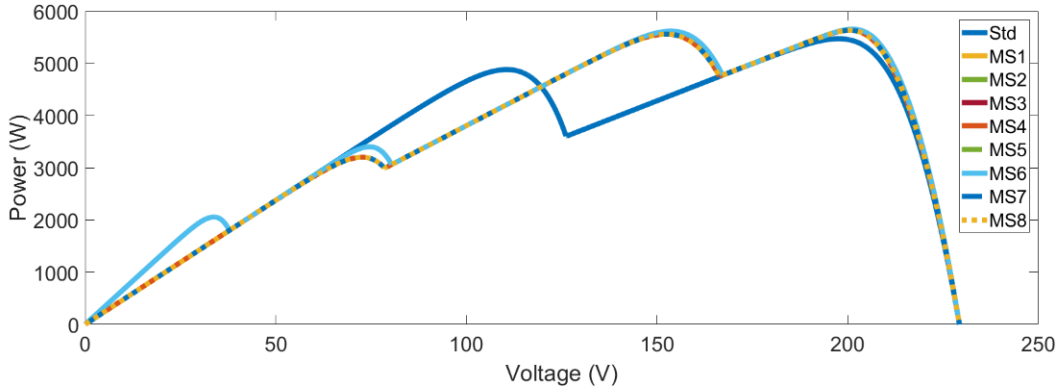

Figure 6.6: Shading test for shadow pattern 1.

reached by the MS configuration is up to 5416W, while the standard configuration reaches 3720W.

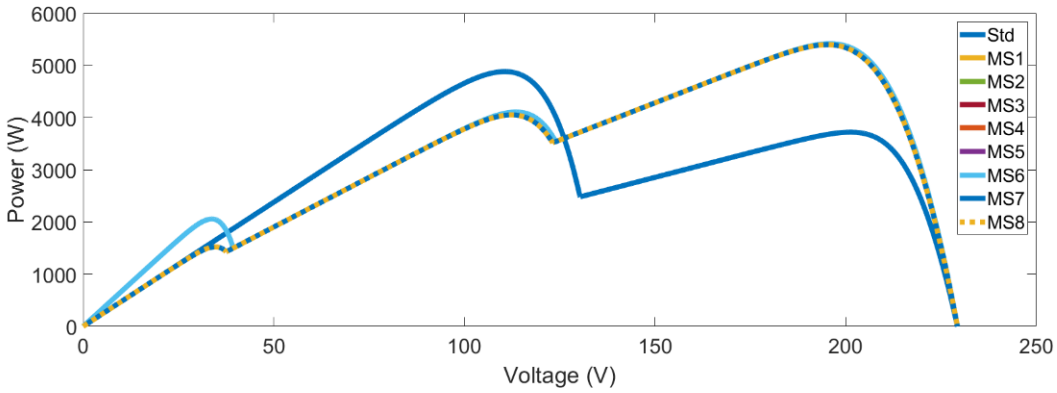

Figure 6.7: Shading test for shadow pattern 2.

The shadow pattern 3 is tested by shading two rows, representing 40% of shaded modules shown in Figure 6.8. In this case, the difference between the MS and the standard configuration is minimal, it is only 3.9%, where the MPP relative to the MS equals 5074W, while the MPP for the standard configuration is equal to 4880W.

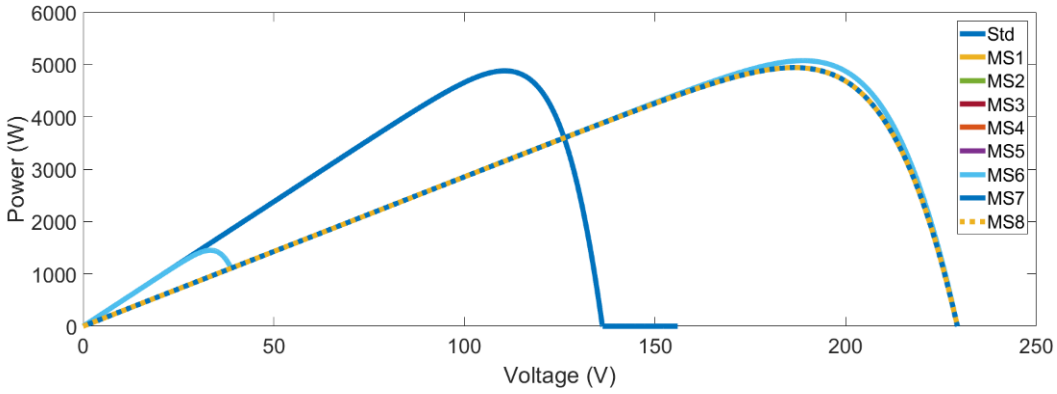

Figure 6.8: Shading test for shadow pattern 3.

The shadow pattern 4 shown in Figure 6.9 behaves similarly with the shadow pattern 3. In this case 56% of the modules are shaded. The MPP difference between the standard and MS configuration is only 6.5%, where the MPP of the MS being equal to 3410W and the standard equal to 3201W.

The eight 5x5 variations for the MS implemented, presented minimal variations in relation to MPP. As shown in Chapter 4, it is known that there is a very high number for different possibilities for a 5x5 MS and depending on the configuration used, the results may be different. However regardless of the configuration used it is possible to reduce losses due to partial shading.

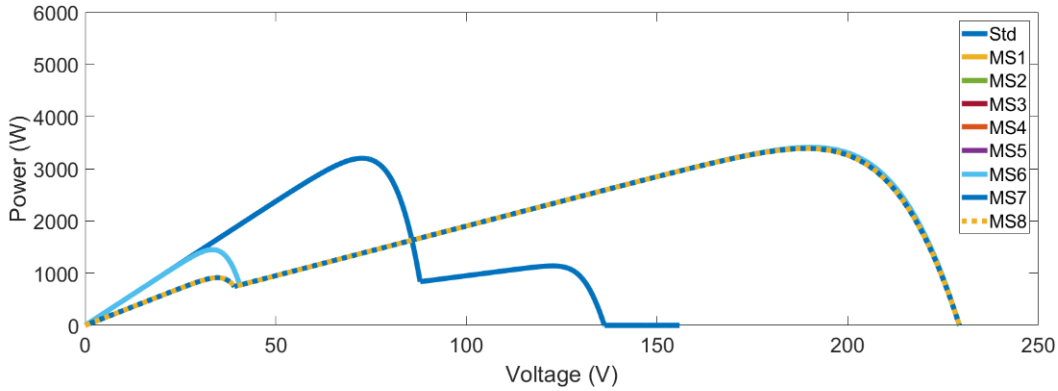

Figure 6.9: Shading test for shadow pattern 4.

The Adaptive P&O was implemented with the 5x5 arrangements presented on Figure 5.3 and 5.4(a), using the same configurations for MS and standard array under shading condition shown in Figure 6.4(c). It is observed in Figure 6.10 that the Adaptive P&O is able to maintain the MPP constant without ripple, unlike a classical P&O. The disadvantage of the MS array Figure 5.4(a) with respect to the original arrangement Figure 5.3 is the transient state which is longer.

As the voltage level for steady state on the original array is smaller than in the MS array, the Adaptive P&O can set the voltage for the MPP at a higher speed. The Adaptive P&O for the MS array works with a higher power level, in addition to a lower working current. The current difference between the standard and MS configuration is 63%, where the current relative to the standard array equals 44A, while the current for the MS array is equal to 27A. This means that when using the MS configuration, it is possible to work with lower currents representing fewer losses due to heating of the conductors. For all tests, the MS presented the advantages of the standard array. Either by a higher MPP or by allowing to operate with a lower current, as shown in this test with the Adaptive P&O.

6.6 Simulations and results for 6x6

In this topic, the power-voltage curves is presented and also the table that presents the values of MPP, VMPP (voltage at the maximum power point) and IMPP (current at the maximum power point) for all tests.

In shadow pattern 1. Figure 6.5(a) the power per voltage response given as in Figure 6.11. The MPP levels are slightly larger for MS1, MS2, and MS4 configurations compared to the standard one, and the MS3, MS5, MS7, and MS8, presented a lot better MPP. The highest and lowest MPP reached by the MS was 5075W and 4601W respectively, whereas for the standard configuration it was 4508W. Thus, up to 12.5% more power with the MS can be obtained than the standard configuration; also the MS works up to 48

The shadow pattern 2 shown in Figure 6.5(b) is simulated when shading 55% of the modules shown in Figure 6.12. In this case, it can be clearly seen that the use of the

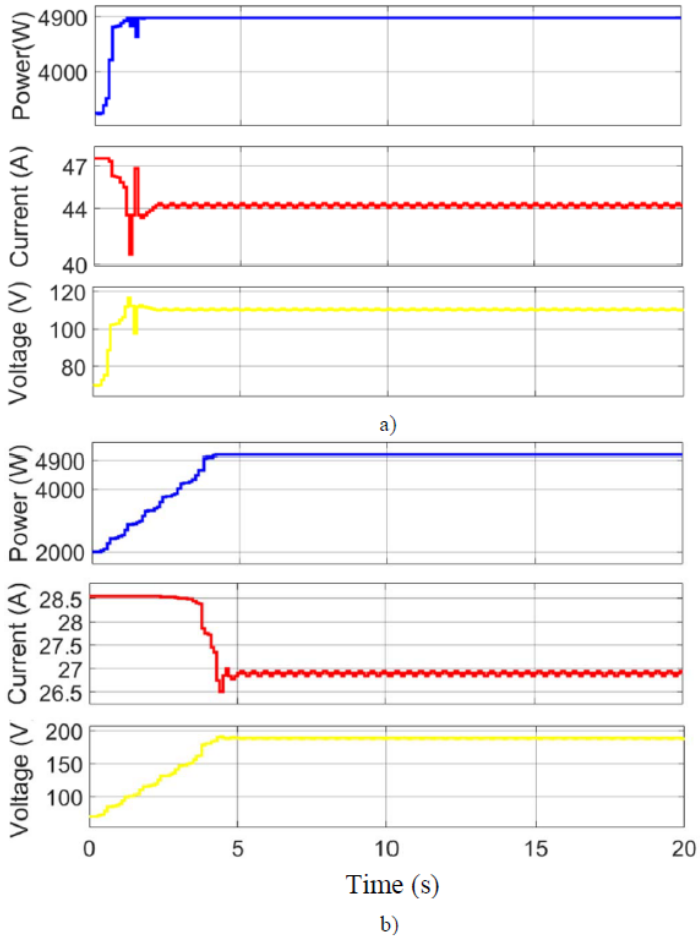

Figure 6.10: Adaptive P&O with MS under partial shading. a) Original array; b) MS array.

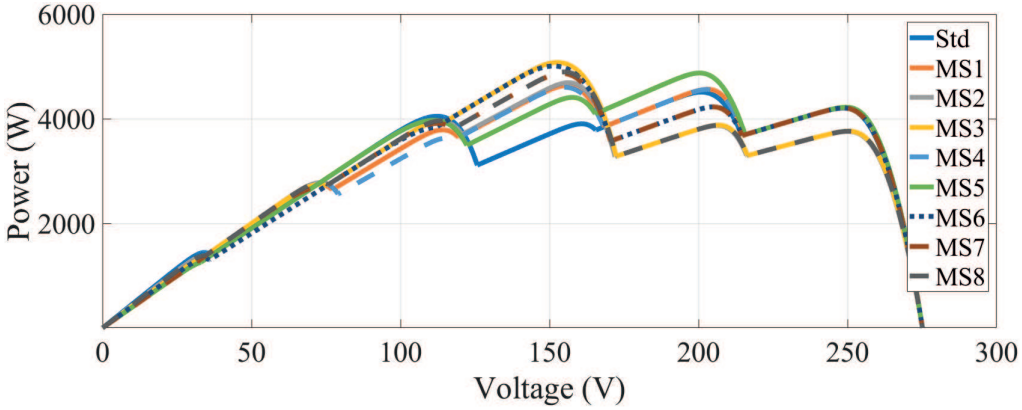

Figure 6.11: Power per voltage curve for shadow pattern 1.

settings with MS are more efficient than the standard setting, reaching up to 17.9% more of MPP and 22.9% more current at this point. The MPP reached by the MS configuration is up to 9106W, while the standard configuration reaches 7719W.

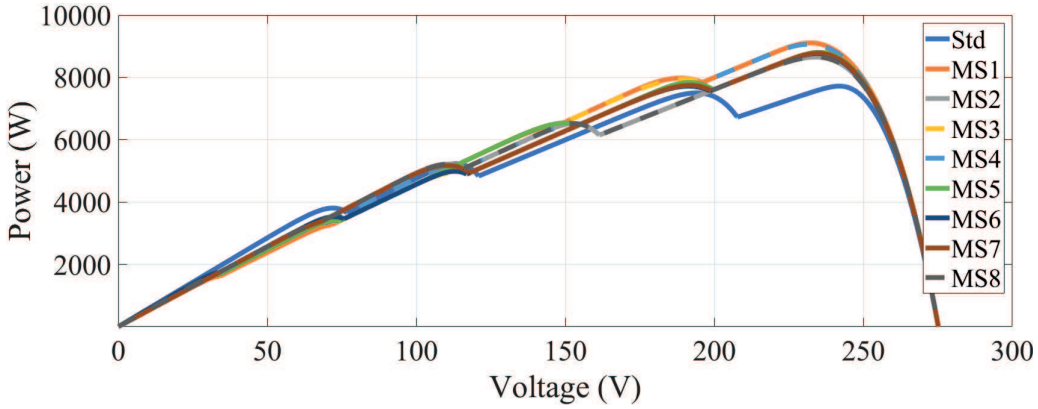

Figure 6.12: Power per voltage curve for shadow pattern 2.

The shadow pattern 3 shown in Figure 6.5(c) is tested by five rows, representing 83% of partially shaded modules shown in Figure 6.13. In this case, there is a high difference in power output between the MS and the standard configuration. The highest MPP is relative to MS1 equal 6069W and the lowest equals to 4622W for MS2 and MS8, while for the standard configuration is only 4088W. It is also observed that the VMPP is lower for the standard array, implicating on a higher operating current. Comparing the best results from MS, the IMPP for the standard configuration is 34% bigger, resulting in a lower MPP and a bigger IMPP. It means that the power difference may be greater if the heat effect on the wires is taken into account.

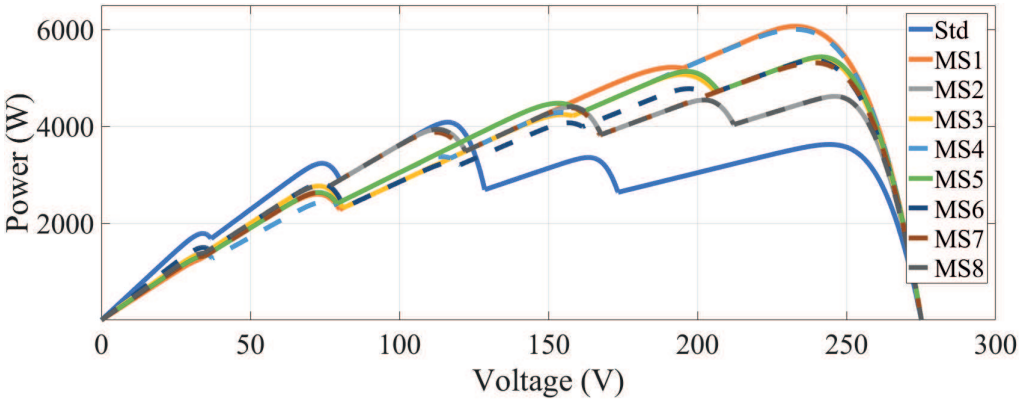

Figure 6.13: Power per voltage curve for shadow pattern 3.

The shadow pattern 4 shown in Figure 6.5(d) results in Figure 6.14, occurring when half of the modules are totally shaded, resulting in a better output for the standard array. In this case, the MPP difference between the standard an MS configuration is up to 37.2%,

while the current differs only 5.8%, where the MPP of the standard being equal to 5929W and the MS varying from 4318W for the MS8 to 5043W for the MS5, MS6 and MS7.

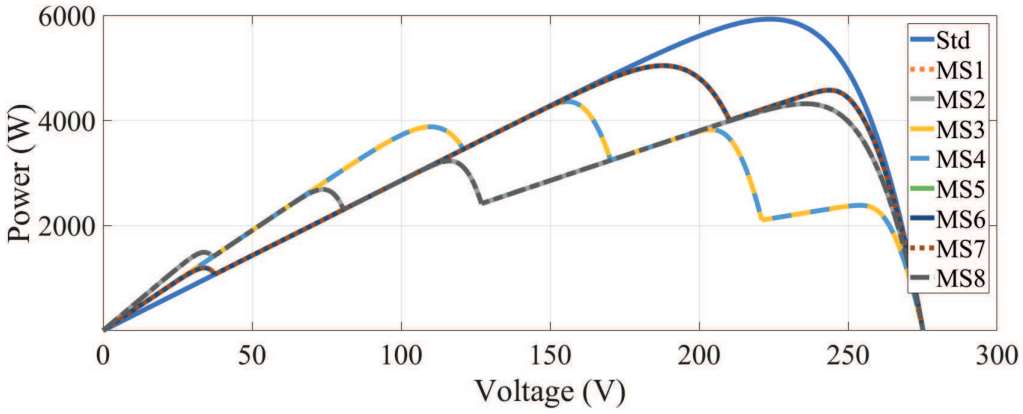

Figure 6.14: Power per voltage curve for shadow pattern 4.

Similar to the shadow pattern 4, the shadow pattern 5 shown in Figure 6.5(e), the standard array shows a better MPP compared to the MS ones shown in Figure6.15. While the MPP for the standard array equals to 7151W, for the MS it varies from 5535 for MS3 and MS4 to 6340 for MS7. Also, the current from the standard array at MPP is 30.5% bigger than the MS with the higher MPP.

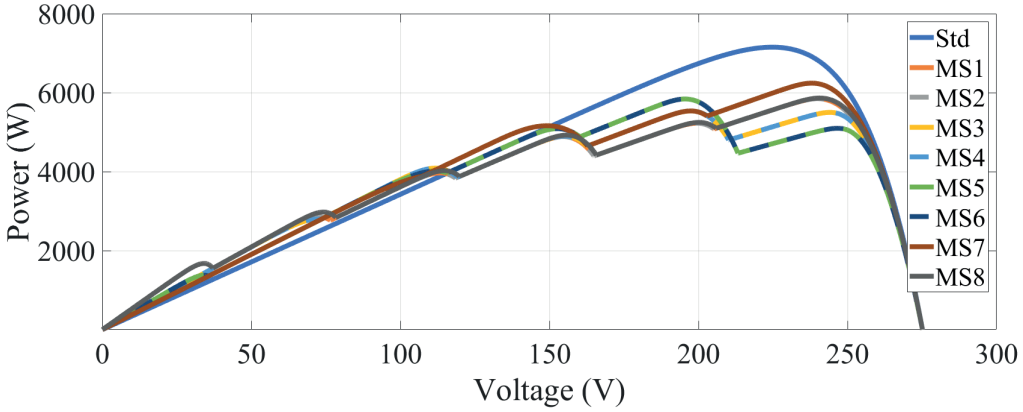

Figure 6.15: Power per voltage curve for shadow pattern 5.

In shadow pattern 6, Figure 6.5(f), is simulated when the bottom four rows are partially shaded, shown in Figure 6.16. The MS configurations are slightly more efficient than the standard setting, with up to 16.6% more MPP. The lowest and highest MPP for the MS arrays are 5535W and 6240W respectively, while the standard array has only 5351 of power output. In this case, voltage on the VMPP is lower for the standard array than the others, implicating on a higher operating current at this point. Similar to the shadow pattern 3, the current from the standard array is bigger than the MS ones even with lower MPP being 28% bigger.

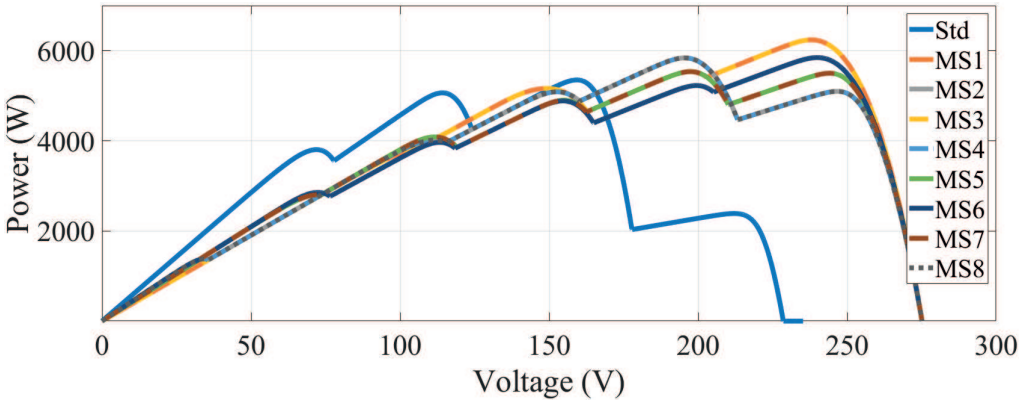

Figure 6.16: Power per voltage curve for shadow pattern 6.

In shadow pattern 7, Figure 6.5(g), 91% of the modules are partially shaded, resulting in Figure 6.17. In this case, the MS configurations can minimize shadow effects a lot better than the standard array with up to 46.2% of more MPP. The highest and lowest values from the MS are 5671W (MS3 and MS7) and 4578W (MS1) respectively. The classic configuration MPP is only 3877W. By comparing the best MPP from MS and the standard configuration, there is only a 0.1% difference between then currents.

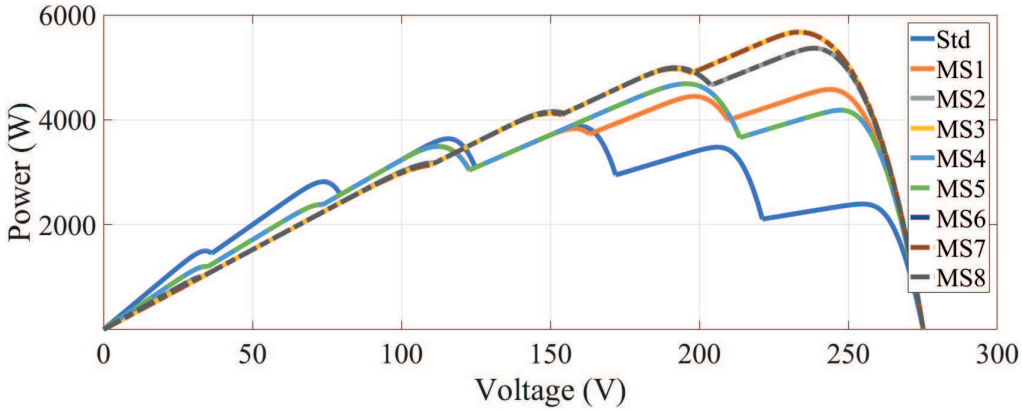

Figure 6.17: Power per voltage curve for shadow pattern 7.

The shadow pattern 8, Figure 6.5(h), is tested by partially shading all the modules on the array, and the results are shown in Figure 6.18. As in the shadow patterns of the shadows 4 and 5, the last shadow pattern has a better result for the standard array, up to 27% more MPP than the MS configurations. While the standard array has 3212W of MPP, the MS ones are varying from 2312W to 2710W. Besides the MPP, the current is also bigger than the MS with the higher MPP, being 25% bigger.

By comparing the tests, there is not a single configuration that can be better than the others in all cases, also shown in Figure 6.19 for comparison. However, depending on the place where the modules are installed might occur a usual type of shadow. In this case, the

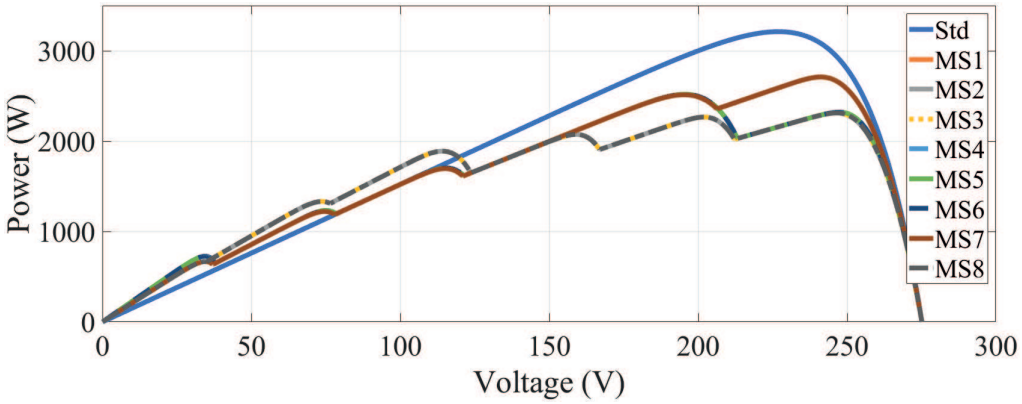

Figure 6.18: Power per voltage curve for shadow pattern 8.

best solution can be implemented. As mentioned on Table 5.1, there is a large number of possibilities of unique MS solutions to be tested on a 6x6 MS, so it is possible to achieve a configuration that has better results than the ones tested in this work.

The graphic shown in Figure 6.19 and the Table 6.2 demonstrate that amongst MS rotations can present a great difference of MPP under the same shadow condition. By comparing the tests, there is not a single configuration that can be better than the others in all cases. As mentioned on Section IV, there is a large number of possibilities of unique MS solutions to be tested on a MS, so there is a great number of 6x6 MS possibilities to obtain different results for any shading pattern.

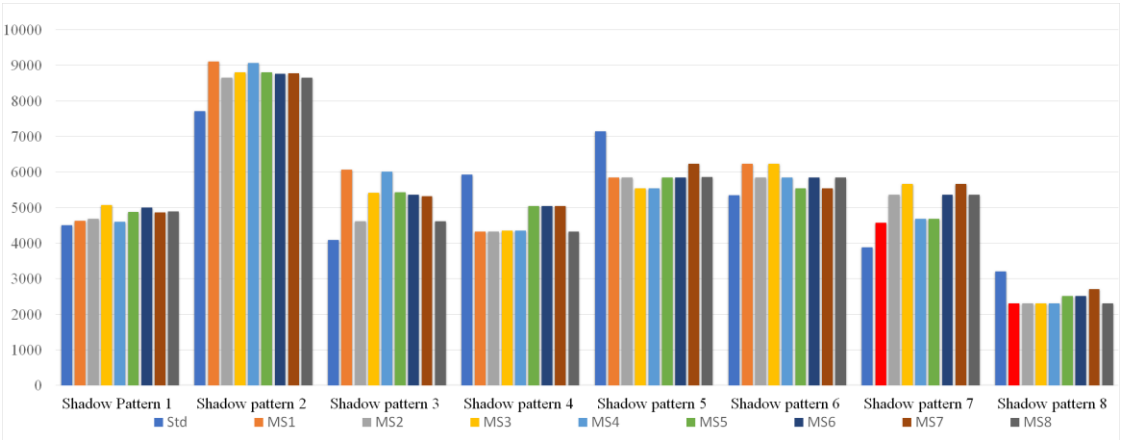

Figure 6.19: The power output for each configuration under shading patterns.

Table 6.2: Results from the 6x6 shadow patterns.

Shadow pattern 1									
	Standard	MS1	MS2	MS3	MS4	MS5	MS6	MS7	MS8
MPP (W)	4508.19	4632.75	4689.08	5075.23	4601.24	4873.16	5006.24	4865.97	4893.46
VMPP (V)	200.87	155.75	165.5	152.62	155.00	200.25	151.37	154.12	154.87
Io (A)	22.44	29.74	28.33	33.25	29.69	24.34	33.07	31.57	31.60
Shadow pattern 2									
	Standard	MS1	MS2	MS3	MS4	MS5	MS6	MS7	MS8
MPP (W)	7719.63	9406.57	8652.57	8811.00	9061.05	8799.42	8764.30	8777.54	8652.57
VMPP (V)	241.87	232.12	233.87	235.25	231.50	235.12	234.37	234.62	233.87
Io (A)	31.92	39.23	37.00	37.45	39.14	37.43	37.40	37.41	37.00
Shadow pattern 3									
	Standard	MS1	MS2	MS3	MS4	MS5	MS6	MS7	MS8
MPP (W)	4088.56	6069.17	4622.12	5417.67	6005.83	5438.16	5368.86	5315.94	4622.12
VMPP (V)	116.25	232.75	246.12	240.75	232.75	241.50	238.87	238.87	246.12
Io (A)	35.17	26.08	18.78	22.50	25.80	22.52	22.48	22.25	18.78
Shadow pattern 4									
	Standard	MS1	MS2	MS3	MS4	MS5	MS6	MS7	MS8
MPP (W)	5929.64	4318.83	4318.83	4359.49	4359.49	5043.51	5043.51	5043.51	4318.83
VMPP (V)	233.75	235.62	235.62	156.00	156.00	187.87	187.87	187.87	235.62
Io (A)	25.37	18.33	18.33	27.95	27.95	26.85	26.85	26.85	18.33
Shadow pattern 5									
	Standard	MS1	MS2	MS3	MS4	MS5	MS6	MS7	MS8
MPP (W)	7151.38	5847.11	5847.11	5847.11	5535.76	5839.70	5839.70	6240.35	5863.64
VMPP (V)	224.75	240.00	240.00	197.37	197.37	195.50	195.50	238.0	240.62
Io (A)	31.82	24.36	24.36	28.05	28.05	29.87	29.87	26.22	24.37
Shadow pattenr 6									
	Standard	MS1	MS2	MS3	MS4	MS5	MS6	MS7	MS8
MPP (W)	5351.30	6240.35	5837.70	6240.35	5837.70	5535.76	5847.11	5535.76	5839.70
VMPP (V)	159.37	238.00	195.50	238.0	195.50	197.37	240.00	197.37	195.50
Io (A)	33.58	26.22	29.87	26.22	29.87	28.05	24.36	28.05	29.87
Shadow pattern 7									
	Standard	MS1	MS2	MS3	MS4	MS5	MS6	MS7	MS8
MPP (W)	3877.26	4578.12	5364.20	5671.29	4686.03	4686.03	5364.20	5671.29	5364.20
VMPP (V)	159.87	243.87	238.50	233.50	195.62	195.62	238.50	233.50	238.50
Io (A)	24.25	18.77	22.49	24.29	23.95	23.95	22.49	24.29	22.49
Shadow pattern 8									
	Standard	MS1	MS2	MS3	MS4	MS5	MS6	MS7	MS8
MPP (W)	3212.05	2312.13	2312.13	2312.13	2312.13	2517.79	2517.79	2710.44	2312.13
VMPP (V)	227.00	246.50	246.50	246.50	246.50	195.50	195.50	241.12	246.50
Io (A)	14.15	9.38	9.38	9.38	9.38	12.88	12.88	11.24	9.38

Chapter 7

Conclusion

7.1 General conclusion

This dissertation presents a 5x5 and a 6x6 MS permutation under different partial shadow conditions compared to a standard array. The MS represents a mathematical puzzle, and the permutation maintains the MS characteristics. The losses caused by shading can be reduced by repositioning the modules in a PV system and based on the simulations, it is also known that MS helps to reduce losses due to shading, but not in all cases.

For the 5x5, in the 4 cases tested, the MS presented gains even when more than 50% of the modules are shaded. The eight different configurations for a single solution of MS shown similar results for all cases tested. Through the comparison made with Adaptive P&O associated with MS and original array, it was possible to confirm that MS can represent smaller losses by working with lower currents to a similar MPP level. The difference between the MS maximum power points rotations was low.

For the 6x6, in five of eight cases tested, the MS presented better results than the standard array, achieving more than 45% MPP in two cases. However, on the other three, the classic configuration was more efficient with the shadow pattern. Besides that, the current at MPP was very different in some cases, which may represent a greater value of voltage drop due to the effect of heat on the conductors. Even MS being most efficient in most of these cases, there is a very high number of unique solutions for a 6x6 MS. Then there may be some combination better than the one unique solution tested.

It is possible to conclude that the bigger the array, the bigger is the difference between the MPP‘s for the MS rotations. Even in the shadow pattern 4 shwon in Figure 6.5(d), where there are only two irradiance levels (just like for the 5x5 shadow patterns), the 6x6 MS presented different MPP’s as shown in Table 6.2. For the 5x5 MS‘s, independently of the shadow pattern, the MPP‘s were almost the same for all cases.

Bibliography

Bessy, B. F. (1699), *Memoires de L'Academie Royale des Sciences*, International Series on Computational Intelligence, Par la Compagnie des Libraries, Paris, pp. 303–354.

Bosco, M. J. & M. C. Mabel (2017), 'A novel cross diagonal view configuration of a pv system under partial shading condition', *Solar Energy* **158**, 760–773.

Castelano, N. N., J. A. G. Parra, J. Valls-Guirado & F. Manzano-Agugliaro (2015), 'Optimal displacement of photovoltaic arrays rows using a novel shading model', *Aplied Energy* **144**, 1–9.

Chen, C., H. Chang, C. Kuo & C. Lin (2013), 'Programmable energy source emulator for photovoltaic panels considering partial shadow effect', *Energy* **54**, 174–183.

Deshkar, S. N., S. B. Dhale, J. S. Mukherjee, T. S. Babu & N. Rajasekar (2015), 'Solar pv array reconfiguration under partial shading conditions for maximum power extraction using genetic algorithm', *Renewable and Sustainable Energy Reviews* **43**, 102–110.

Dhimish, M., V. Holmes, B. Mehrdadi, M. Dales, B. Chong & L. Zhang (2015), 'Seven indicators variations for multiple pv array configurations under partial shading and faulty pv conditions', *Renewable Energy* **113**, 438–460.

Fahrenbruch, A. L. & R. H. Bube (1983), 'Fundamentals of solar cells: Photovoltaic solar energy conversion', *Elsevier* **1**, 9–10.

Ishaque, K. & Z. Salam (2013), 'Review of maximu poewr point tracking techniques of pv system for uniform insolation and partial shading condition', *Renewable and Sustainable Energy Reviews* **19**, 475–488.

Kabir, E. & P. Kumar (2018), 'Solar energy: Potential and future prospects', *Energy Reviews* **82**, 894–900.

Kalogirou, A. S. (2014), 'Fundamentals of solar cells: Photovoltaic solar energy conversion', *Elsevier* **2**, 20–24.

Kardi, R., H. Andrei, J. Gaubert, T. Ivanovici, G. Champeonis & P. Andrei (2012), 'Modeling of the photovoltaic cell circuit parameters for optimum connection model and real-time emulator with partial shadow conditions', *Energy* **42**, 57–67.

Loly, P., I. Cameron & W. Trump (2009), 'Magic square spectra', *Linear Algebra and its Applications* **430**, 2659–2680.

Malathy, S. & R. Ramaprabha (2018), 'Reconfiguration strategies to extract maximum power from photovoltaic array under partially shaded conditions', *Renewable and Sustainable Energy Reviews* **81**, 2922–2934.

Muthuramalingam, M. & P. S. Manoharan (2014), 'Comparative analysis of distributed mppt controllers for partially shaded stand alone photovoltaic systems', *Energy Conversion and Management* **86**, 286–299.

Nguyen, X. H. (2015), 'Matlab/simulink based modeling to study effect of partial shadow on solar photovoltaic array', *Enviromental Systems Research* pp. 4–20.

Pendem, S. R. & S. Mikkili (2018), 'Modelling and performance assessment of pv array topologies under partial shading conditions to mitigate the mismatching power losses', *Solar Energy* **160**, 303–321.

Pinn, K. & C. Wieczerkowski (1998), 'Number of magic squares from parallel tempering monte carlo', *International Journal of Modern Physics* **4**, 541–546.

Schroeppel, R. (1976), 'The order 5 magic squares program', *Scientific American* .

Sharma, A. K., R. Dwivedi, S. K. Srivastava & C. M. Pathak (1994), 'Performance analysis of a modified solar array under shadow conditions', *Renewable Energy* **4**(2), 257–260.

Silvestre, S., A. Boronat & A. Chouder (2009), 'Study of by-pass diodes configuration on pv modules', *Aplied Energy* **86**, 1632–1640.

Trejos-Grisales, L. A., C. A. Ramos-Paja & A. J. Saavedra-Montes (2015), 'Equivalent circuits for simulating irregular pv arrays under partial shading conditions', *Tecno. Lógicas* **18**(35).

Vijayalekshmy, S., G. R. Bindu & S. R. Iyer (2015), 'Analysis of various photovoltaic array configurations under shade dispersion by su do ku arrangement during passing cloud conditions', *Indian Journal of Science and Technology* **8**.

Vijayalekshmy, S., G. R. Bindu & S. R. Iyer (2016), 'A novel zig-zag scheme for power enhancement of partially shaded solar arrays', *Solar Energy* **135**, 92–102.

Villalva, M. G. & E. F. Ruppert (2009), 'Analysis and simulation of the p&o mppt algorithm using a linearized pv array mode', *35th Annual Conferenc of IEE Industrial Electronics* pp. 231–236.

Yadav, A. S., R. K. Pachauri, Y.K. Chauhan, , S. Choudhury & R. Singh (2017), 'Performance enhancement of partially shaded pv array using novel shade dispersion effect on magic-square puzzle configuration', *Solar Energy* **144**, 780–797.